ANL/LWRS-21/1

Effect of thermal aging and irradiation on microstructure and crack growth response of Alloy 690

LWRS milestone Report Number: M3LW-21OR0402039

Nuclear Science and Engineering Division
Argonne National Laboratory

About Argonne National Laboratory
Argonne is a U.S. Department of Energy laboratory managed by UChicago Argonne, LLC under contract DE-AC02-06CH11357. The Laboratory's main facility is outside Chicago, at 9700 South Cass Avenue, Argonne, Illinois 60439. For information about Argonne and its pioneering science and technology programs, see www.anl.gov.

DOCUMENT AVAILABILITY

Online Access: U.S. Department of Energy (DOE) reports produced after 1991 and a growing number of pre-1991 documents are available free at OSTI.GOV (http://www.osti.gov/), a service of the US Dept. of Energy's Office of Scientific and Technical Information.

Reports not in digital format may be purchased by the public from the National Technical Information Service (NTIS):
U.S. Department of Commerce
National Technical Information
Service 5301 Shawnee Rd
Alexandria, VA 22312
www.ntis.gov
Phone: (800) 553-NTIS (6847) or (703) 605-6000
Fax: (703) 605-6900
Email: **orders@ntis.gov**

Reports not in digital format are available to DOE and DOE contractors from the Office of Scientific and Technical Information (OSTI):
U.S. Department of Energy
Office of Scientific and Technical Information
P.O. Box 62
Oak Ridge, TN 37831-0062
www.osti.gov
Phone: (865) 576-8401
Fax: (865) 576-5728
Email: **reports@osti.gov**

Disclaimer
This report was prepared as an account of work sponsored by an agency of the United States Government. Neither the United States Government nor any agency thereof, nor UChicago Argonne, LLC, nor any of their employees or officers, makes any warranty, express or implied, or assumes any legal liability or responsibility for the accuracy, completeness, or usefulness of any information, apparatus, product, or process disclosed, or represents that its use would not infringe privately owned rights. Reference herein to any specific commercial product, process, or service by trade name, trademark, manufacturer, or otherwise, does not necessarily constitute or imply its endorsement, recommendation, or favoring by the United States Government or any agency thereof. The views and opinions of document authors expressed herein do not necessarily state or reflect those of the United States Government or any agency thereof, Argonne National Laboratory, or UChicago Argonne, LLC.

ANL/LWRS-21/1

Effect of thermal aging and irradiation on microstructure and crack growth response of Alloy 690

LWRS milestone Report Number: M3LW-21OR0402039

Bogdan Alexandreanu, Yiren Chen, Xuan Zhang and Wei-Ying Chen

Nuclear Science and Engineering Division, Argonne National Laboratory

September 2021

This page intentionally left blank

ABSTRACT

Nickel-base Alloy 690 and the associated weld Alloys 52 and 152 are typically used for nozzle penetrations in replacement heads for pressurized water reactor (PWR) vessels, because of their excellent overall resistance to general corrosion and environmental degradation, primarily stress corrosion cracking (SCC). However, many of the existing PWRs reactors are expected to operate for 40-80 years. Likewise, advanced water-cooled small modular reactors (SMRs) will use Ni-Cr alloys and are expected to receive initial operating licenses for 60 years. Hence, the thermal stability of Ni-Cr alloys is a potential concern for the long-term performance of both existing and advanced nuclear plants, and possibly spent fuel storage containers. The objective of this research is to understand the microstructural changes occurring in high-Cr, Ni-based Alloy 690 during long time exposure to the reactor operating temperatures, and the effect of these changes on the service performance. One area of particular concern is the potential for long range ordering (LRO), *i.e.* formation of the intermetallic Ni_2Cr phase under prolonged exposure to reactor temperatures and/or irradiation, which can increase strength, decrease ductility, and cause dimensional changes or lead to in-service embrittlement of components made with these alloys. Hence, this research focused on the microstructural evolution and the SCC response of Alloy 690 under accelerated thermal aging and irradiation conditions. The materials studied involved Alloy 690 from two sources: (i) Alloy 690 plate from an Alloy 152 dissimilar metal weld (DMW) joining the Alloy 690 plate to Alloy 533 LAS, aged at three different temperatures (370°C, 400°C and 450°C) for up to 75,000h (equivalent to 60 years of service), and (ii) specimens neutron-irradiated in the BOR-60 reactor up to 40 dpa. For aged Alloy 690 specimens, hardness was found to increase with aging time, however, the microstructural characterization by means of synchrotron X-ray did not find evidence of LRO. The microstructural characterization of neutron-irradiated specimens by TEM found no evidence of LRO either. Testing in a primary water environment of Alloy 690 specimens aged to a 60-year service equivalent revealed a fatigue and corrosion fatigue crack growth responses similar to those measured on the un-aged alloy. The SCC CGR response was also low. Overall, the two Alloy 690 heats investigated in this work, aged up to 60-year service equivalents or exposed to neutron irradiation up to 40 dpa, did not exhibit a deterioration in microstructure or performance.

TABLE OF CONTENTS

LIST OF FIGURES

LIST OF TABLES

ABBREVIATIONS

ANL	Argonne National Laboratory
APS	Advanced Photon Source
ASTM	American Society for Testing and Materials
BPR	Back Pressure Regulator
BWR	Boiling Water Reactor
CGR	Crack Growth Rate
CL	Constant Load
CMTR	Certified Material Test Report
CSL	Coincident Site Lattice
CT	Compact Tension
DO	Dissolved Oxygen
DMW	Dissimilar Metal Weld
ECP	Electrochemical Potential
EDX	Energy Dispersive X-ray Spectroscopy
EPRI MRP	Electric Power Research Institute Materials Reliability Program
GBE	Grain Boundary Engineering
GTAW	Gas Tungsten Arc Welding
HAZ	Heat Affected Zone
HX	Heat Exchanger
IG	Intergranular
LAS	Low Alloy Steel
LWR	Light Water Reactor
NRC	Nuclear Regulatory Commission
PPU	Partial Periodic Unloading
PWR	Pressurized Water Reactor
PWHT	Post Weld Heat Treatment
PWSCC	Primary Water Stress Corrosion Cracking
SCC	Stress Corrosion Cracking
SEM	Scanning Electron Microscopy
SMAW	Shielded Metal Arc Welding
SS	Stainless Steel
S	Side
T	Transverse
TC	Thermocouple
TG	Transgranular
WOL	Weld Overlay
WPS	Weld Procedure Specification

ACKNOWLEDGMENTS

This research was supported through the U.S. Department of Energy's Light Water Reactor Sustainability program. Program managers: Dr. Thomas. M. Rosseel and Dr. Xiang (Frank) Chen.

1 Introduction

Nickel-based Alloy 690 and the associated weld Alloys 52 and 152 are typically used for nozzle penetrations in replacement heads for pressurized water reactor (PWR) vessels, because of their increased resistance to stress corrosion cracking (SCC) relative to Alloys 600, 82, and 182 [1, 2]. Many of these reactors are expected to operate for 40-80 years. Likewise, advanced water-cooled small modular reactors (SMRs) will use Ni-Cr alloys in their primary systems and are expected to receive initial operating licenses for 60 years. For spent fuel containers, the desired lifetime is 10,000 years. Hence, the thermal stability of Ni-Cr alloys is a potential concern for the long-term performance of nuclear plants and possibly spent fuel storage containers.

One area of concern is that the long time exposure to reactor operating temperatures can result in long range ordering (LRO), *i.e.* formation of the intermetallic Ni_2Cr phase which can lead to in-service embrittlement of Ni-Cr components. Research with binary Ni-Cr binary alloys by Young et al [3] have found that LRO promotes SCC, with an SCC CGR 1,000x larger than the non-ordered version of the alloy. However, Fe plays a key role in ordering, and it is not clear at this time whether LRO occurs in commercial heats as the addition of Fe was found to hinder LRO formation [4].

Perhaps the most comprehensive study on LRO of Alloy 690 was conducted by Framatome/ EdF [5, 6]. One of the main findings of this study was that an Alloy 690 heat with 7.2 wt. % Fe requires 70,000 h to develop LRO at 420°C, while ordering had not occurred in Alloy 690 with 10.4 wt. % Fe aged for 70,000 h at the same temperature. 20% added cold-work was found to decrease the time to develop LRO slightly, to 60,000h. More recently, Huotilainen et al. found significant increases in hardness in two of the four heats aged up to 10,000h at 400°C [7]. The two heats that hardened had a lower Fe content than the heats that did not harden as a result of aging (9.53 and 9.3 wt. % vs. 10.37 and 10.04 wt. %). The latter observation is consistent with the formation of LRO as its kinetics are known to decrease with Fe concentration, however, Fe levels of up to 10 wt. % were found not to impede the LRO formation [4]. Nevertheless, the hardening reported in two of the four heats is similar to that resulting from 15-20% added cold work [7], thus, may have the potential to lead to moderate SCC CGRs, comparable to those typical of Alloy 600. Another remarkable recent study has found that LRO precipitation under proton irradiation was observed for the first time, in alloys C22, 625, 625P, 625D, 725, and 690 [8]. The Fe level in the Alloy 690 heat was 10.38 wt. %, and the irradiation was conducted at 360°C with 2 MeV protons to a damage level of 2.5 dpa.

Overall, the research to date on the effect of aging in Ni-based alloys seems to have been focused almost exclusively on the base alloys, and primarily on model alloys as the investigators sought to gain a fundamental understanding of the mechanisms in play. As a result, research on commercial heats has been extremely scarce and limited to microstructural examinations. As noted previously, with the notable exception of the study by Young et. al [3] on model alloy Ni-33Cr, the effects of those microstructural changes on the SCC response have not been evaluated.

The need for an assessment of the long-term aging effects on the performance in Alloy 690 and associated weldments was identified as a research gap in the Light Water Reactor Sustainability (LWRS) stakeholders report for 2020 [9], and was recognized as a strategic research need by both industry [2, 10] and regulators [11]. Hence, the research undertaken in this project aims to address that need, and bridge the gap between the microstructural examination and performance testing. In order to study the effect of aging on performance, ANL produced an Alloy 152 dissimilar metal weld joining Alloy 690 and Alloy 533 LAS in 2011, identical to the one developed and produced for the US NRC program in 2010, which was then aged up to 75,000h over the following nine years, to 30 and 60-year service equivalents. This creates the opportunity to examine the effects of aging in several pedigreed alloys that have been characterized and tested extensively at ANL and worldwide in the un-aged condition over the past decade.

Chapter 2 describes the weld mockup used in the aging study, including the materials of fabrication, the schematic design of the welds, and the weld fabrication processes. One of the objectives for this weldments was that the materials and welding parameters be representative of those used for actual welds used in service. In addition, prompted by the results presented in [8] where protons were found to induce LRO, Alloy 690 specimens irradiated in the BOR-60 reactor and tested at ANL under the US NRC program, were re-examined to investigate whether neutron irradiation can also induce LRO. Chapter 2 also presents the equipment used in the microstructural examinations. The crack growth testing equipment and experimental approach are also presented. ANL generally followed a well-established testing protocol that has been employed for a number of years and was reported in previous ANL reports.

Chapter 3 provides findings of the microstructural examinations and the results of the crack growth rate tests. Complete CGR data sets are provided as a function of testing conditions, and presented as crack advance vs. time plots.

Chapter 4 provides a discussion of the testing results in the framework provided by the well-established fatigue and corrosion fatigue behavior for these alloys, as well as the industry-proposed disposition curves for crack growth [1]. Finally, Chapter 5 gives a summary of the main findings and conclusions.

2 Experimental

This section describes the alloys used in this study, the equipment used for microstructural analysis, the configuration of test specimens for crack growth rate (CGR) testing, and the CGR test apparatus and experimental approach.

2.1 Alloys

The alloys used in this work came from two sources: i) aged Alloy 690 plate, part of a weldment that was aged to 30-year and 60-year service equivalents, and ii) Alloy 690 specimens neutron-irradiated in the BOR-60 reactor up to 40 dpa. Since the focus of the study was LRO, model alloy Ni-33Cr – with known susceptibility to LRO - was also included in the investigation.

2.1.1 Alloy 690 to Alloy 533 Grade B Joint (Alloy 152 weld produced by ANL)

The research presented in this report focuses on aged Alloy 690 which was part of a weldment, hence, for completeness, this section presents the all the component materials and steps undertaken to produce the weldment.

The Alloy 690 (Heat NX3297HK12) was received from Nuclear Alloy Corp. in a plate form that was 6.4-cm (2.25-in.) thick x 7.6-cm (3-in.) wide x 86.4-cm (34-in.) long. The designation for the metallurgical condition of the as-received plate was MIL-DTL-24802. To reach this condition, the alloy was vacuum-induction-melted, electro-slag-remelted, hot-rolled, de-scaled, and annealed at 1038°C (1900°F) for 2 h, then air-cooled. The chemical composition provided by the vendor, as well as that determined at ANL by inductively-coupled plasma optical emission spectrometry (ICP-OES), is reported in Table 1.

Table 1 Chemical composition (wt.%) of Alloy 690 (Heat NX3297HK12) plate.

Alloy ID (Heat)	Analysis	C	Mn	Fe	S	P	Si	Cu	Ni	Cr	Ti	Nb	Co
A 690WC (NX3297HK12)	Vendor	0.03	0.20	9.9	<0.001	-	0.07	0.01	59.5	29.5	-	-	-
	ANL	0.04	0.33	8.53	0.001	0.003	0.02	0.04	59.67	30.82	0.47	0.01	<0.01

The Alloy 690 plate was used to produce a 3-inch thick Alloy 152 butt weld to SA-533 Gr B class 1 steel (Heat A5466-2 from the Midland reactor lower head [12]) buttered with Alloy 152 filler metal. The geometry of the joint is shown in Figure 1. The joint was designed with a straight edge on the Alloy 690 side to facilitate SCC CGR testing of the Alloy 690 heat affected zone (HAZ). The SMAW welding procedure was qualified to ASME Section IX by ANL Central Shops [13].

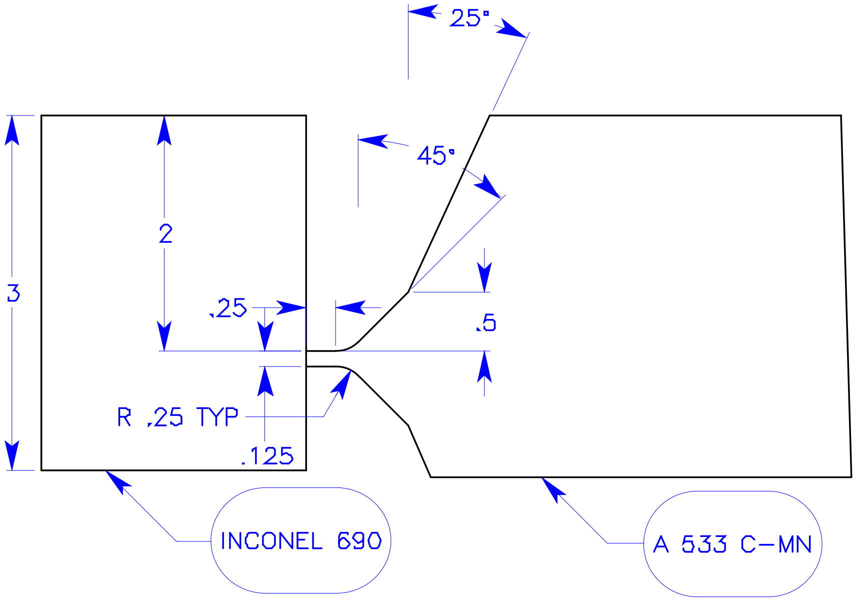

Figure 1 Joint design, Alloy 690 to SA-533 Gr B. Units are in inch.

2.1.1.1 Alloy 152 Weld Buttering

The LAS plate was machined with a bevel on one end. The beveled end was buttered with Alloy 152 F43 filler metal. A record was kept of the number and location of weld passes together with the heat code of the filler metal used, and the welding parameters that were used, Table 2 [13]. This record is shown in [13]. After each layer, a liquid penetrant (LP) check was performed. After buttering, the LAS piece was stress relieved at 1150 ± 25ºF for 3h. The chemical composition of the Alloy 152 filler heat 720129 that was used to produce the first layer of buttering is given in Table 3.

Table 2 Welding process and conditions for various weld passes used for fabricating the Alloy 152 butter

Weld Pass	Process	Filler Metal	Filler Size, in.	Heat Code	Type Polarity	Current, A	Voltage, V	Travel Speed, in./min	Notes
1 – 23	SMAW	Alloy 152, EniCrFe-7	1/8	720129	DCRP	97-102	21 – 23	5	Layer 1 LP
24-44	SMAW	Alloy 152, EniCrFe-7	5/32	146444	DCRP	113-117	25 – 26	5	Layer 2 LP
45-65	SMAW	Alloy 152, EniCrFe-7	5/32	146444	DCRP	113-117	25 – 26	5	Layer 3 LP

DCRP = direct current reverse polarity

Table 3 Chemical composition (wt.%) of Alloy 152 heats used to produce the weld buttering

Alloy ID	Analysis	C	Mn	Fe	S	P	Si	Cu	Ni	Cr	Ti	Nb+Ta	Co
A152 (720129)	CMTR	0.037	3.70	9.28	<0.001	<0.003	0.51	0.01	55.26	28.92	0.12	1.92	<0.01
A152 (146444)	CMTR	0.040	3.56	9.36	<0.001	<0.003	0.46	<0.01	55.25	29.04	0.15	1.84	<0.01

2.1.1.2 Alloy 152 Butt Weld

The buttered LAS piece described in the previous sub-section was beveled on the buttered edge leaving ¼” of Alloy 152 F43 weld material on the face, and a section of Alloy 690 plate was used to make the opposing part of the butt weld. A double bevel J-grove weld was produced according to the design shown in Figure 1, and the number and location of weld passes together with the heat code of the filler metal used, as well as the welding parameters are given in Table 4. The root pass of the weld and back grind was LP tested, and the final weld surface was also LP tested. The final weld was radiographed per ASME Section IX. The resulting weld along with its component heats is shown in Figure 2. The chemical composition of the Alloy 152 filler heat WC04F6 that was used to complete the butt weld is given in Table 5.

Table 4 Welding process and conditions for various weld passes used for fabricating the A152 butt weld

Weld Pass	Process	Filler Metal	Filler Size, in.	Heat Code	Type Polarity	Current, A	Voltage, V	Travel Speed, in./min	Notes
1 – 8	SMAW	Alloy 152, EniCrFe-7	1/8	720129	DCRP	97-102	21 – 23	5	
9-14	SMAW	Alloy 152, EniCrFe-7	1/8	146444	DCRP	97-102	25 – 26	5	Root LP BG LP
15-26	SMAW	Alloy 152, EniCrFe-7	5/32	146444	DCRP	113-117	25 – 26	5	Final LP
27-76	SMAW	Alloy 152, EniCrFe-7	1/8	WCO4F6	DCRP	97-102	25 – 26	5	Final LP

DCRP = direct current reverse polarity

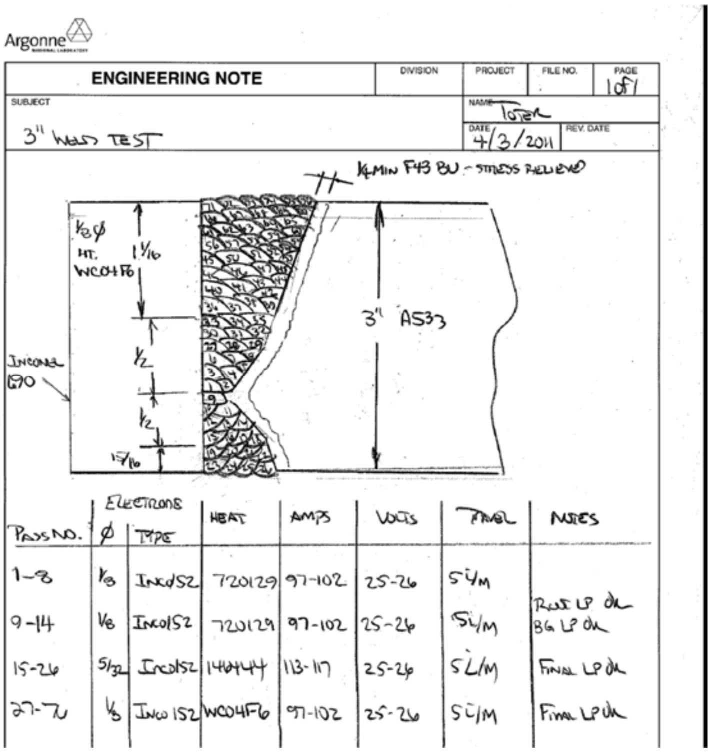
Argonne

ENGINEERING NOTE	DIVISION	PROJECT	FILE NO.	PAGE 1of1

SUBJECT 3" WELD TEST
NAME Toter
DATE 4/3/2011
REV. DATE

PASS NO.	ELECTRONS ∅	TYPE	HEAT	AMPS	VOLTS	TRAVEL	NOTES
1-8	1/8	INCO152	720129	97-102	25-26	5"/M	
9-14	1/8	INCO152	720129	97-102	25-26	5"/M	ROOT LP OK BG LP OK
15-26	5/32	INCO152	146444	113-117	25-26	5"/M	FINAL LP OK
27-76	1/8	INCO 152	WC04F6	97-102	25-26	5"/M	FINAL LP OK

Figure 2 **Schematic of the Alloy 152 weld joining Alloy 690 and Alloy 533 produced for aging in 2011. The weld was produced in an identical fashion using the same materials and procedures used to produce the weld for the US NRC program a year earlier. The table below the weld schematic shows the Alloy 152 weld heats and welding parameters.**

Table 5 Chemical composition (wt.%) of Alloy 152 heat WC04F6 used to complete the butt weld

Alloy ID (Heat)	Analysis	C	Mn	Fe	S	P	Si	Cu	Ni	Cr	Ti	Nb	Co
A152 (WC04F6)	CMTR	0.048	3.48	10.39	0.003	0.003	0.41	<0.01	55.20	28.70	0.09	1.54	<0.005
	ANL	-	3.88	9.56	-	<0.08	0.52	<0.04	53.70	28.40	0.10	1.80	<0.04

2.1.2 Prior characterization and testing of the un-aged Alloy 690 to Alloy 533 Grade B Joint

One of the main advantages of using the weldment described in this section for an aging study is the existence of a large database for benchmarking. The non-aged material from the sister weldment have been tested extensively at ANL under an US NRC program [14-16] and elsewhere. Some key findings are as follows:

Alloy 690:

- Alloy 690 Heat NX3297HK12 was the original material used by ANL in 2006 to show that 26% cold work promotes SCC growth in Alloy 690. The material was shared with several other laboratories and was tested extensively worldwide. Notably, 11% - the most from any one heat - of the data points in the MRP-386 database [2] were obtained using this heat. Alloy 690 Heat NX3297HK12 has a Fe content below 10 wt. % (9.9 and 8.53 wt. % in two independent measurements, Table 1), so it could be prone to developing LRO under long term exposure.

The Alloy 152 weldment was produced with three heats:

- Alloy 152 Weld Heat WC04F6 was used in the upper J-weld. It was tested extensively at ANL [14, 16] and elsewhere, and significant IG SCC was developed routinely in testing. It is the most SCC-susceptible weldment in the MRP-386 database [2]. Alloy 152 Weld Heat WC04F6 has a Fe content of 10.39 wt. % (Table 5), so it would be less prone to the formation of LRO under long term exposure.
- Alloy 152 Weld Heat 720129 was used to weld on both sides of the root. It has not been tested as part of the weld, but was tested as the first buttering layer on Alloy 533 LAS. Alloy 152 Weld Heat 720129 has a Fe content of 9.28 wt. % (see Table 3), so it would be prone to LRO formation under long term exposure.
- Alloy 152 Weld Heat 146144 was used to complete the bottom J-weld. It has not been tested as part of the weld, but was tested as the second buttering layer on Alloy 533 LAS. Alloy 152 Weld Heat 146144 has a Fe content of 9.36 wt. % (see Table 3), so it would be prone to LRO formation under long term exposure.

The Alloy 152 butter was produced with two heats (Table 3):

- Alloy 152 Weld Heat 720129 was used as a first layer butter on Alloy 533 LAS. It has been tested extensively at ANL [15] and elsewhere. In SCC CGR testing, this weldment produced fully IG-engaged crack fronts, and very high rates [15]. The weldment and tested specimens were examined extensively at ANL and worldwide. Alloy 152 Weld Heat 720129 has a Fe content of 9.28 wt. % (see Table 3), so it would be prone to LRO formation under long term exposure.
- Alloy 152 Weld Heat 146144 was used as a second layer butter on the Alloy 533 LAS and was tested in that configuration. This weldment was found to be resistant. Alloy 152 Weld Heat 146144 has a Fe content of 9.36 wt. % (see Table 3), so it would be prone to LRO formation under long term exposure.

This weldment was also made available to collaborators from Korea, and the microstructure of the Alloy 152 weld, particularly the butter, was examined extensively in the non-aged and intermediate aged conditions [17, 18].

2.1.3 Aging of the Alloy 690 to Alloy 533 Grade B Joint

In order to emulate the thermal exposure at temperatures of 320°C during 30-year and 60-year service lifetimes of a component, this study employed an accelerated aging approach. The aging conditions were determined using the following equation:

$$\frac{t_{aging}}{t_{ref}} = \exp\left[-\frac{Q}{R}\left(\frac{1}{T_{ref}} - \frac{1}{T_{aging}}\right)\right] \tag{1}$$

where t_{aging} is the aging time (h), t_{ref} is the service time at operation temperature (h), T_{aging} is aging temperature (K), T_{ref} is operation temperature (K), R is the gas constant, and Q is the activation energy.

The 30-year and 60-year year service equivalents were estimated for three aging temperatures (370°C, 400°C, and 450°C) using Eq. (1) with an activation energy of 125 kJ/mol, in excellent agreement with the Framatome/EdF estimate for LRO formation [6], and the results are shown in Figure 3. The figure also includes a photograph of the actual aged weld pieces. The maximum accelerated aging temperature was 450°C to prevent the formation of microstructural phases atypical of normal operating conditions, such as excessive carbides or sigma phases. Specimens are designated by “temperature – service equivalent”, for example specimen “400-Y60” was aged at a temperature of 400°C to reach a 60-year equivalent exposure at 320°C.

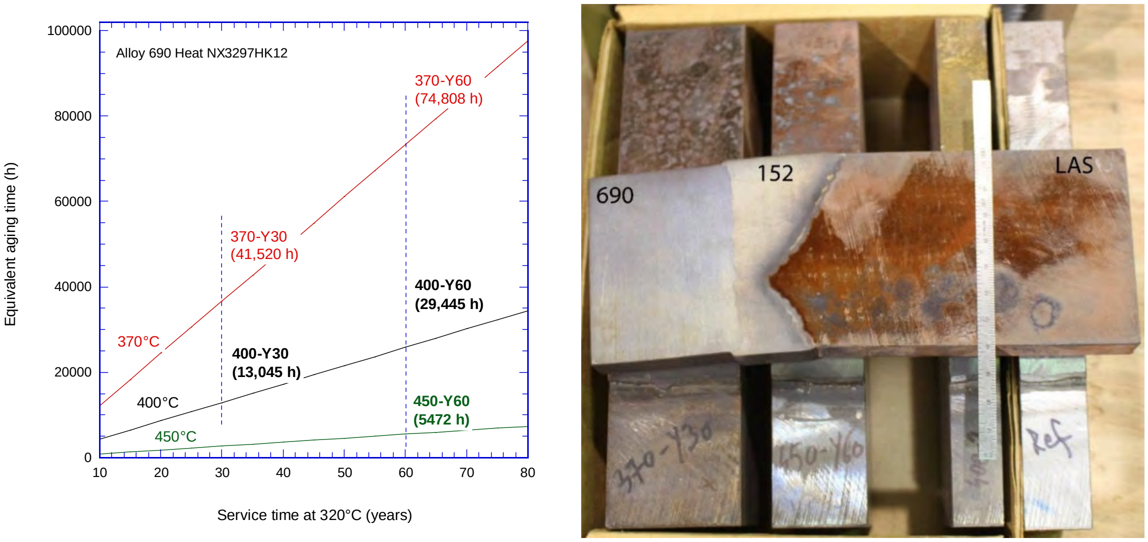

(a) (b)

Figure 3 **(a) Diagram showing the total hours for each aging temperature (370°C, 400°C, and 450°C). Estimates for 30-year and 60-year service equivalents calculated using Eq. (1) with an activation energy of 125 kJ/mol. The diagram also includes the actual aging times. (b) photograph of the actual pieces of Alloy 152 weld joining Alloy 690 and Alloy 533 that were aged.**

2.1.4 Neutron-irradiated Alloy 690

The chemical compositions of the Alloy 690 alloys that were irradiated in the BOR-60 reactor are provided in Table 6. One heat was Grain Boundary Engineered (GBE), a theremo-mechanical processing used to increase the proportions of low energy, SCC-resistant [19] Coincident Site Lattice (CSL) grain boundaries. The first heat, 690 GBE, has a Fe content of 10.26 wt. % which makes it comparable to that used in [8], in which proton irradiation of 2.5 dpa at 360°C was found to induce LRO. The Fe level in the second Alloy 690 heat, 690 BASE, was 9.02 wt. %, so it would also be prone to LRO formation under long term thermal exposure.

Table 6 Chemical composition (wt.%) of the Alloy 690 heats irradiated in BOR-60 reactor

Heat ID	Addtl. Processing	Code	C	Fe	S	P	Si	Ni	Cr
690 GBE	GBE	E1	0.010	10.26	0.003	-	0.030	59.40	29.10
690 BASE	none	E2	0.030	9.02	<0.01	-	0.005	61.49	29.24

GBE = Grain Boundary Engineered

Irradiation of Alloy 690 was conducted in the BOR-60 reactor, a sodium-cooled fast breeder reactor located in the Research Institute of Atomic Reactor (RIAR), Dimitrovgrad, Russia. TEM disks concealed in four weeper capsules were irradiated to 5, 10, 20 and 40 dpa, respectively, during Boris-6 and -7 irradiation experiments. The Boris-6 irradiation included 8 irradiation sub-cycles and several shut-down periods, and the Boris-7 irradiation had 6 irradiation sub-cycles. The irradiation experiments were conducted in the fifth row of the reactor core. Neutron fluence was monitored with 5 dosimeters loaded in the central channel of the irradiation rig along with the specimens. The analyses of these dosimeters were carried out by RIAR after irradiation. The sample temperature during irradiation was controlled by the inlet and outlet sodium, which was kept at 315 and 325°C, respectively. Magnesium-Zinc eutectic thermal monitors were also placed among the samples, confirming that the peak irradiation temperature did not exceed 343°C.

2.1.5 Prior characterization and testing of the neutron-irradiated Alloy 690

Along with the TEM samples, small tensile samples of Alloy 690, with and without prior GBE treatment, were also irradiated to ~5 and 10 dpa in the BOR-60. These samples were tested at ~315°C in simulated PWR coolant with a nominal strain rate of 7.4 10^{-7} s^{-1} (Figure 4). No elevated IASCC susceptibility was detected among these samples in the test environment. The yield stress and the ultimate tensile strength of GBE 690 were slightly lower than that of Alloy 690 at both doses. The total elongation of GBE 690 was also ~10% and ~5% greater than its non-GBE counterparts at 5 and 10 dpa, respectively. The dominant fracture mode of all samples was ductile dimples, suggesting a good IASCC resistance of these alloys in the test environment.

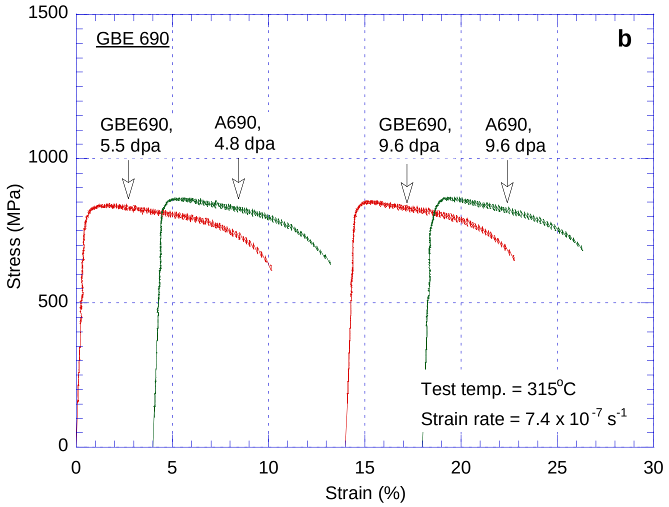

Figure 4 **Stress-vs.-strain curves of Alloy 690 in PWR water at 315°C.**

2.1.6 Model Ni-33Cr Alloy

Given that model alloys tend to develop LRO readily (see for example ref. [3]), a piece of model alloy with demonstrated LRO history [20] was obtained for this program from one of the authors, Dr. S.S. Kim of KAERI, Korea. The Ni-33Cr plate was made by vacuum induction melting followed by hot rolling at 1200°C, solution annealing at 1050°C for 1 h and water quenching. At ANL, this solution-annealed alloy was subjected to two different aging treatments at 475°C known to induce LRO [3]. The intent is to use these conditions as reference for the material characterization effort undertaken in this program which involves commercial heats.

2.2 Microstructural Characterization

The microstructural characterization involved hardness testing as well as analytical techniques such as diffraction at ANL APS or in a TEM focusing on detecting LRO.

2.2.1 X-ray Diffraction at Argonne APS

X-ray diffraction experiments were undertaken at ANL APS with the purpose of detecting LRO in aged Alloy 690 specimens. A similar evaluation has been undertaken previously at ANL APS on a model Ni-33Cr alloy where LRO occurs readily, in as little as 240h under thermal exposure of 475°C [20]. For example, Figure 5 (taken from ref. [20]) shows synchrotron X-ray diffraction peaks from Ni-33Cr alloy in water-quenched and aged conditions. The initial portions of the respective spectra are magnified and are shown as inserts in each figure. In addition to the expected FCC peaks that are present in all alloy conditions, figures (c) and (d) exhibit peaks - indexed with red – typical of Pt_2Mo-type domains. These Pt_2Mo superlattice peaks with d-spacings of 3.76 Å, 3.24 Å, and 2.38 Å were indexed as the (020), (011), and (110) of the BCO structure, and indicate the occurrence of Pt_2Mo-type ordering, i.e., LRO in aged samples.

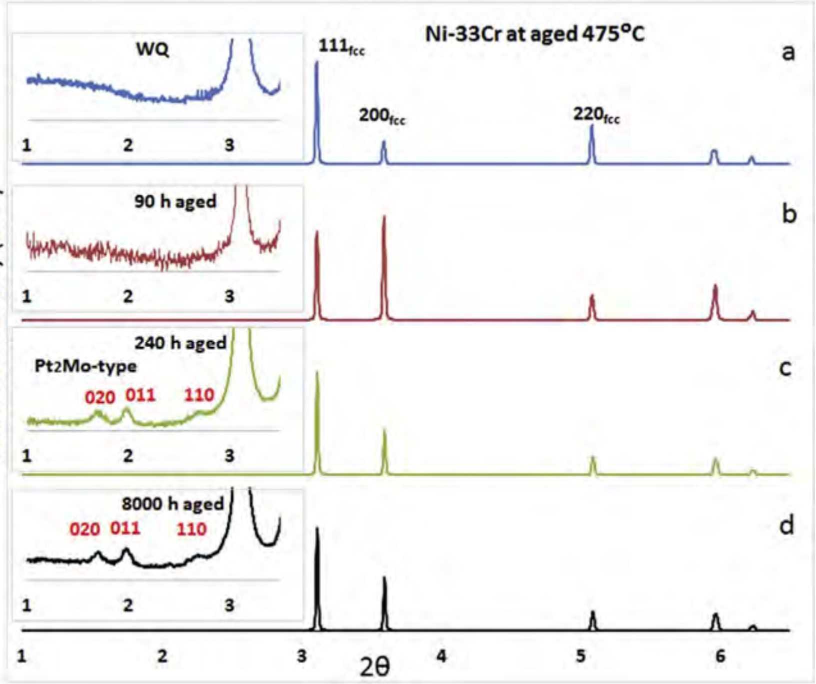

Figure 5 Synchrotron X-ray peaks from Ni-33Cr alloy (a) water-quenched alloy (b) 90 h aged (c) 240 h aged (d) 8000 h aged. Initial portions of the respective spectra are magnified and are shown as insets. In addition to the FCC peaks that are present in all alloy conditions, (c) and (d) show peaks (indexed with red) from Pt_2Mo-type domains (taken from ref. [20]).

For the present research, the X-ray diffraction experiments at the ANL APS involved two beam sessions at the 1-ID beamline, and the experimental details are summarized in Table 7. The detectors were calibrated with either a CeO_2 powder sample (NIST standard SRM674b) or a LaB_6 standard sample (NIST standard SRM660B). All the samples were nominally 1-mm thick. For each sample, 100 exposures were made while the sample was continuously moved. The 100 frames were then averaged. This approach maximized the number of grains that the beam sampled to create powder-like diffraction patterns for high-fidelity data analysis. The 2D patterns were transformed into intensity maps of azimuth angles versus radial positions, and were integrated in the azimuthal direction to create the 1-D diffraction profiles for phase identification.

Table 7 Experimental details for the X-ray diffraction conductucted at ANL APS on aged Alloy 690 specimens

Material	Sample condition	Detector	Sample to detector distance (mm)	X-ray energy (keV)	Beam size (mm^2)
Alloy 690	reference	Pilatus3X CdTe 2M	950	71.676	0.2 × 0.2
Alloy 690	400-Y60	Pilatus3X CdTe 2M	950	71.676	0.2 × 0.2
Alloy 690	450-Y60	Pilatus3X CdTe 2M	950	71.676	0.2 × 0.2
Alloy 690	370-Y60	GE-41RT	837	71.676	0.2 × 0.2
Alloy 690	370-Y60 HAZ	GE-41RT	837	71.676	0.2 × 0.2

2.2.2 *TEM*

The neutron-irradiated 3-mm disks of Alloy 690 were electrochemically polished to obtain TEM thin foils. A twin-jet polisher (TenuPol-5) from Struers was used for polishing. The electrolyte was a methanol solution containing 5% perchloric acid. The polishing process was carried out in two steps. First, the 3-mm TEM disk was loaded in a sample holder and thinned to about 100-150 µm thick in the polisher. Then, the disk was perforated at the disk center to generate a wedged area transparent to electron beam. The optimal polishing condition for this material was -30°C, 25 V, and ~100 mA. After polishing, the TEM foils were cleaned and transferred to the IVEM facility for characterization.

A Hitachi-H9000 TEM operated at 300 keV was used to characterize the polished Alloy 690 specimens. The samples were imaged with the bright-field (BF), dark-field (DF), and rel-rod DF imaging techniques for irradiation defects. To search for LRO, selected area diffraction patterns were taken in zone axes, and the presence of superlattice reflections was considered as the evidence of LRO. In addition, the samples were also examined with a through-focus technique to see if voids were generated by the neutron irradiation in Alloy 690 at PWR-relevant temperature.

2.3 PWSCC Crack Growth Rate Testing

2.3.1 Compact tension (CT) Specimens

The tests conducted under this project were performed on ½-T compact tension (CT) specimens; the geometry of the CT specimens is shown in Figure 6. The CGR tests were conducted in simulated PWR environments at 320°C. The testing protocol was in accordance with ASTM E-647, “Standard Test Method for Measurement of Fatigue Crack Growth Rates,” [21] and ASTM E-1681, “Standard Test Method for Determining a Threshold Stress Intensity Factor for Environment-Assisted Cracking of Metallic Materials under Constant Load” [22].

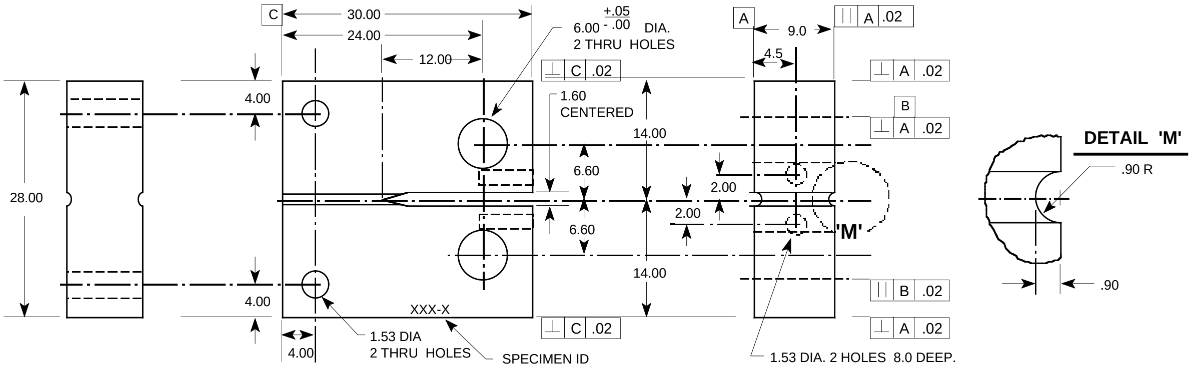

Figure 6 Configuration of the ½-T CT specimen used for this study. Dimensions are in mm.

2.3.2 PWSCC Crack Growth Test Facilities

The CGR tests were conducted in test facilities equipped with either 2 or 6-liter stainless steel (SS) autoclaves. Each system has a suite of calibrated instrumentation, including digitally controlled hydraulic loading and load cells, and an independent water loop to maintain a simulated PWR environment with water chemistry monitoring. The test systems are nearly identical except for the maximum load rating of the test frame and the volume of the autoclave vessel. A detailed description of the test system with the 2-liter autoclave is provided in this section.

The 2-liter autoclave test facility allows test temperatures of up to 350°C. Figure 7 is a photograph showing the entire test system. The servo-hydraulic test frame consists of a load train, an autoclave support frame, and autoclave. The hydraulic actuator is mounted on bottom of the test frame, with the load train components located above it. The load cell is located at the bottom of the pull rod. An Instron Model 8800 system is used to control the load on the specimen. The test temperature is maintained by heater bands mounted on the autoclave body.

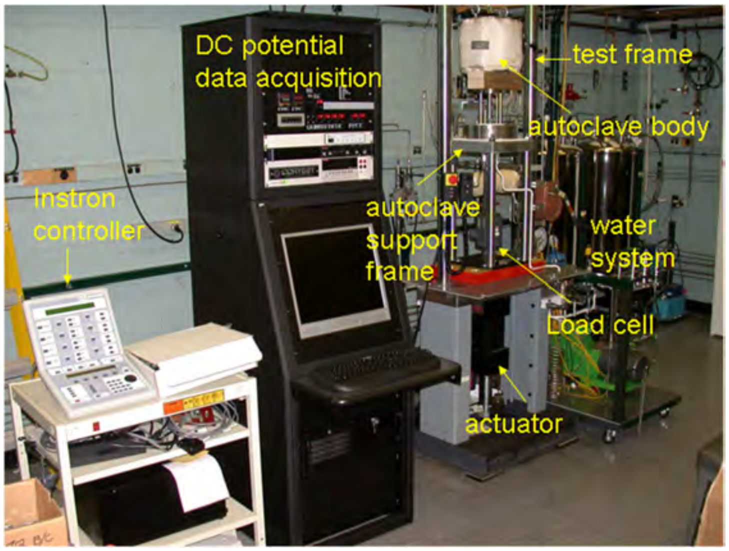

Figure 7 **Layout of the 2-liter SCC test system.**

The autoclave support frame consists of a thick plate supported by four compression rods (Figure 8). The internal load frame that contains the test specimen consists of a top plate supported by three rods. The upper two-piece clevis assembly is fastened to the top plate of the internal load frame, and the lower piece clevis assembly is connected to the pull rod. The specimen to be tested is mounted between the clevises. The specimen and clevises are kept electrically insulated from the load train by using oxidized Zircaloy pins and mica washers to connect the clevises to the rest of the load train. Water is circulated through a port in the autoclave head, which serves both as inlet and outlet. A schematic diagram of the recirculating water system is shown in Figure 9.

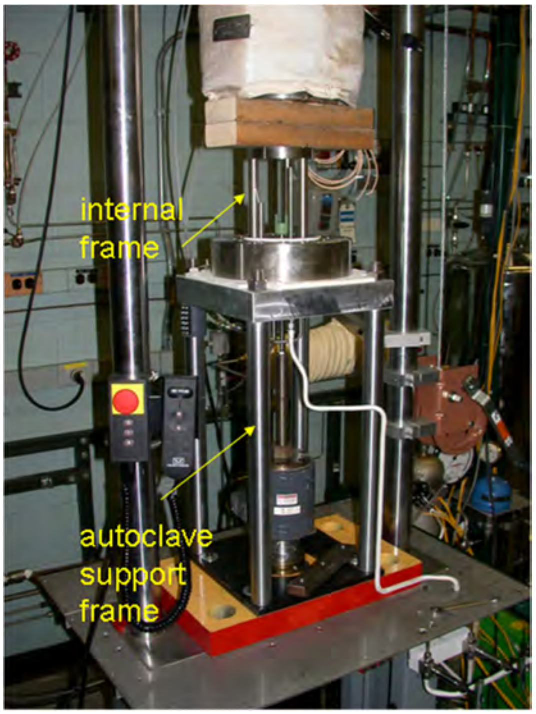

Figure 8 **Photograph of the specimen load train for the 2-liter autoclave**

The simulated PWR feedwater contains 2 ppm Li as LiOH, 1000 ppm B as HBO_3, ≈2 ppm dissolved hydrogen (≈23 cm^3/kg), and less than 10 ppb dissolved oxygen (DO) [23]. Water is circulated at relatively low flow rates (15-25 mL/min). The test temperature was 320°C.

Crack extensions are monitored by the reversing-direct current (DC) potential difference method, Figure 10. In this method, a constant DC current is passed through the test specimen and the crack length is measured through the changes in the electrical voltage at the crack mouth. The electrical voltage measured across the crack mouth is related to the unbroken crack ligament resistance through the Ohm's law. Thus, as the crack advances, the length of the unbroken ligament decreases and its resistance increases. In short, as the crack advances the voltage measured across the crack mouth increases. Figure 10 shows a typical configuration of a CT specimen instrumented for crack growth measurements by the DC potential method: the current leads are welded on the top and bottom surfaces of the specimen, and potential leads are welded on the front face of the specimen across the machined notch but on diagonal ends. Also, to compensate for the effects of changes in resistivity of the material with time, an internal reference bar of the same material being tested is installed in series, near the test specimen. The voltage readings across the reference bar are used to normalize potential drop measurements for the CT test specimen. The changes in potential drop measurements for the CT test specimen are transformed into crack advance data using correlations developed for the specimen geometry that is tested. In practice, voltage readings are taken successively as the current is reversed, and, typically, 800 voltage readings are needed to generate 1 crack advance data point, approximately every 4 min. with a resolution of approximately 1-2 µm [0.039-0.079 mils].

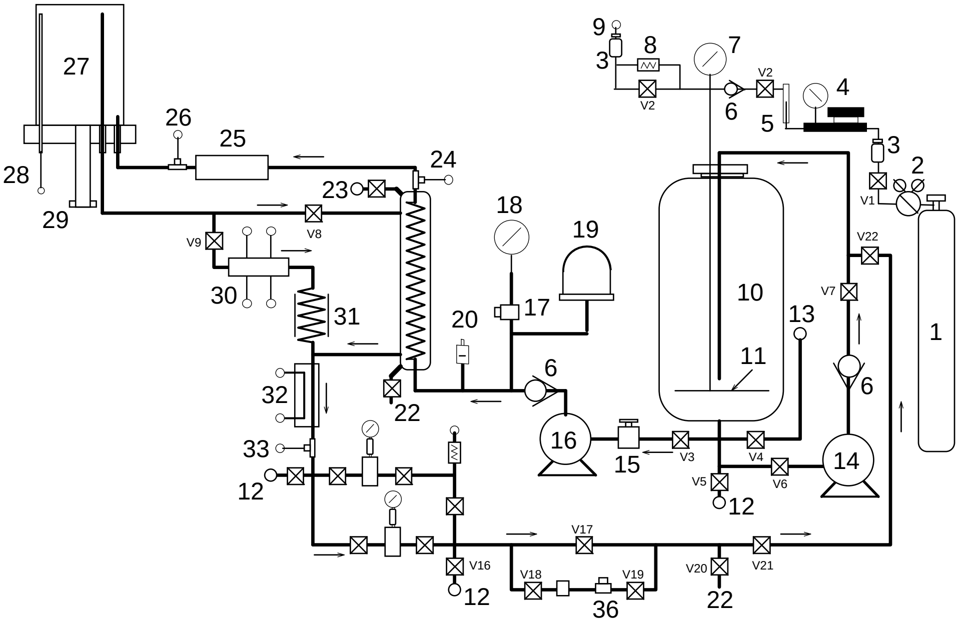

1. COVER GASS SUPPLY TANK
2. TWO-STAGE HIGH-PRESSURE REGULATOR
3. FLASH ARRESTOR
4. LOW-PRESSURE REGULATOR
5. FLOW METER
6. CHECK VALVE
7. COMPOUND VACUUM & PRESSURE GAUGE
8. PRESSURE RELIEF VALVE
9. VENT TO AIR & FLASH ARRESTOR
10. FEEDWATER STORAGE TANK
11. SPARGE TUBE
12. WATER SAMPLE PORT
13. FEEDWATER FILL PORT
14. FEEDWATER TANK RECIRCULATION PUMP
15. SOLENOID VALVE
16. HIGH-PRESSURE PUMP
17. PRESSURE TRANSDUCER
18. HIGH-PRESSURE GAUGE
19. ACCUMULATOR
20. RUPTURE DISC
21. HEAT EXCHANGER (HX)
22. DRAIN
23. SYSTEM BLEED PORT
24. HEAT EXCHANGER OUTLET TC
25. AUTOCLAVE PREHEATER
26. PREHEATER OUTLET TC
27. COMMERCIAL AUTOCLAVE
28. THERMOWELL
29. “BAL SEAL” RETAINER
30. ECP CELL
31. AIR-COOLED COIL
32. WATER COOLED HEAT EXCHANGER
33. BACK-PRESSURE REGULATOR (BPR) INLET TC
34. BPR
35. PH METER
36. CONDUCTIVITY METER

Figure 9 **Schematic diagram of the recirculating 2-liter autoclave system.**

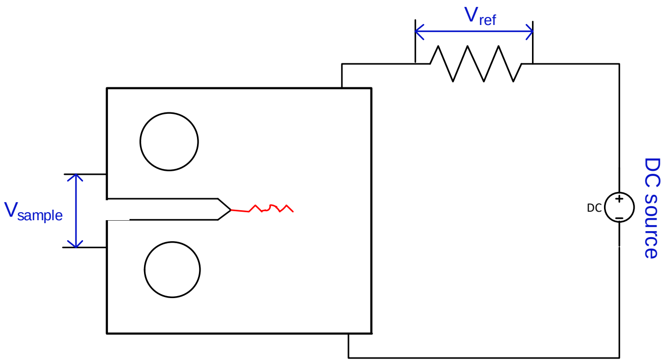

Figure 10 **Principle of crack length measurement by the DC potential method.**

3 Results

This section describes the results of hardness testing of the as-received and aged alloy conditions, the findings on the microstructure examination by X-ray diffraction and TEM, and the results of SCC CGR testing in a primary water environment. The last subsection contains descriptions for two tests on aged specimens, both aged to 60-year service equivalents: one conducted with under alternate funding (Specimen 400-Y60), and one conducted under this program (Specimen 370-Y60).

3.1 Microstructure

3.1.1 Hardness

The hardness of each aged condition of Alloy 690 Heat NX3297HK12 is shown with blue on the "aging time equivalent vs. service time at 320°C" diagram in Figure 11. The load for all measurements was 100 gf, and the standard deviation for each sample hardness average shown in the figure is approximately 6 HV. The plot shows similar increases for all aging temperatures, with the possible exception of 370-series specimens, where hardness appears to decrease with additional aging beyond 370-Y30 condition. The causes for the hardening – either Cr carbide precipitation or LRO – are both known to increase susceptibility to SCC.

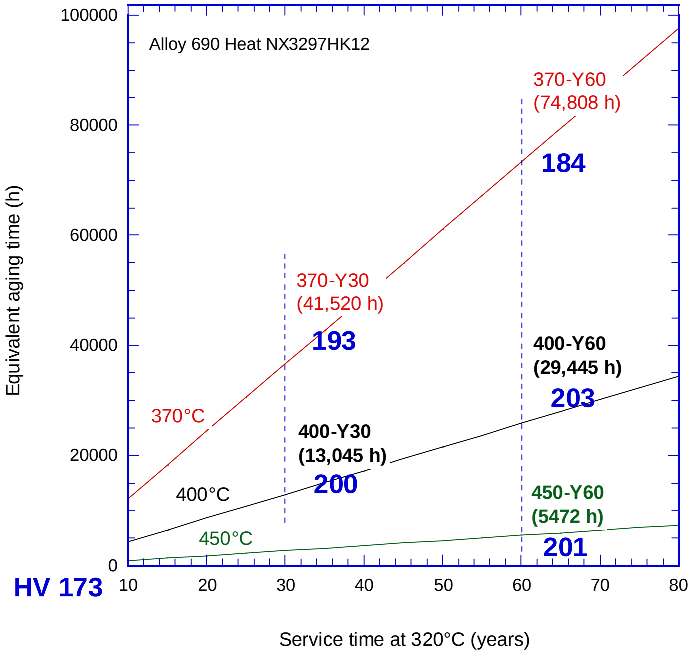

Figure 11 **Hardness for each aged condition is shown with blue on the aging time equivalent vs. service time at 320°C diagram. The standard deviation for each sample hardness average shown in the figure is approximately 6 HV.**

3.1.2 X-ray Diffraction at Argonne APS

X-ray diffraction experiments were conducted at the ANL APS with the purpose of detecting LRO formation.

Figure 12 shows the X-ray diffraction for all conditions aged to 60-year service equivalents, and one observes that no new peaks occur in the aged materials. The same can be observed in the resulting spectra shown at the bottom of the picture. As described previously in Section 2.2.1, Pt_2Mo superlattice peaks with d-spacings of 3.76 Å, 3.24 Å, and 2.38 Å would have been expected to appear in the spectra had Pt_2Mo-type ordering occurred; in the absence of these peaks, the finding is that no LRO occurred in the aged samples.

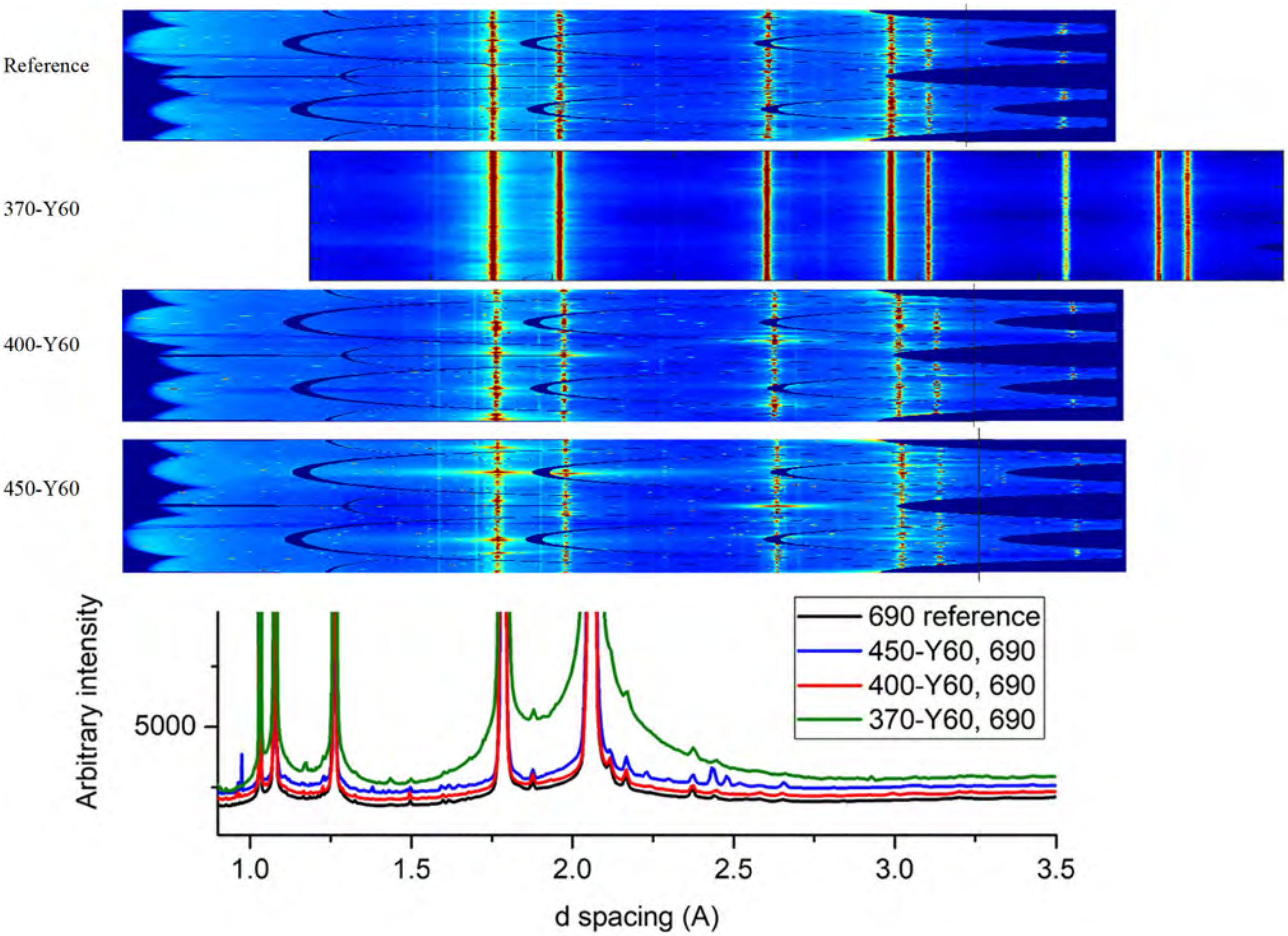

Figure 12 X-ray diffraction for reference non-aged and all conditions aged to 60-year service equivalents. The randomly scattered and relatively weak spots in the patterns - except the 370-Y60 - are from the diffraction of the X-ray harmonic and do not indicate the existence of new phases. The minor peaks in the diffraction patterns are from the TiN and the $Cr_{23}C_6$ phases.

In addition to the above analysis, a modest attempt was made to detect LRO in the HAZ of the weld – an area with increased residual stress and diffusivity. Figure 13 shows X-ray diffraction spectra for aged Alloy 690 condition 370-Y60 at the weld HAZ and away from the HAZ (“base”). As with the previous figure, the absence of Pt_2Mo superlattice peaks suggests that LRO did not occur in either specimen.

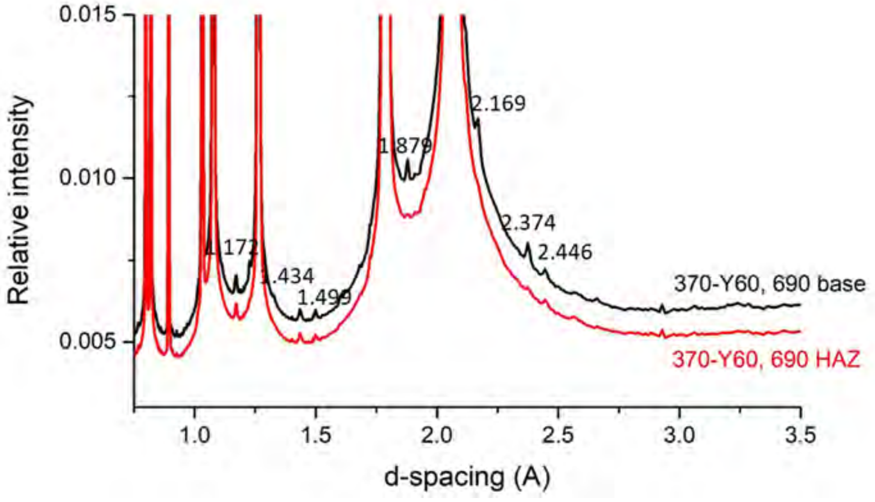

Figure 13 X-ray diffraction spectra for aged Alloy 690 condition 370-Y60 at the weld HAZ and away from the HAZ ("base"). Minor peaks in the diffraction patterns are from the TiN and the $Cr_{23}C_6$ phases.

3.1.3 TEM of Irradiated Alloy 690 Specimens

The TEM characterization was conducted with the purpose of detecting LRO formation in irradiated specimens for which transfer to the ANL APS was not possible under ANL's Limited Operations guidelines due to the Covid-19 pandemic.

The TEM examination matrix is shown in Table 8. In addition to the irradiated alloys, the model alloy Ni-33Cr aged for 2,000h at 475°C with LRO confirmed to occur [20] was included as well as an Alloy 690 specimen (commercial heat) that was aged alongside the model alloy.

Table 8 **TEM examination matrix**

Dose (dpa)	Ni-33Cr, aged[1]	A690, aged[2]	690BASE[3]	690GBE[3]
0	√	X		
5				X
10				X
40			X	X

[1] Model alloy Ni-33Cr was aged for 2,000h at 475°C (LRO confirmed to occur)
[2] Alloy 690 aged for 2,000h at 475°C (commercial companion for the model alloy)
[3] GBE = Grain Boundary Engineered; both conditions of this heat were SCC-tested previously

Figure 14 shows the Diffraction pattern from the model Ni-33C aged for at 475°C for 2,000h. The superlattice reflections (green arrow) confirm the presence of LRO. By contrast, Figure 15 shows the Diffraction patterns from Alloy 690 irradiated to 5 dpa, 10 dpa, and 40 dpa. The absence of superlattice reflections suggests that LRO did not occur with the neutron irradiation in the BOR-60 reactor.

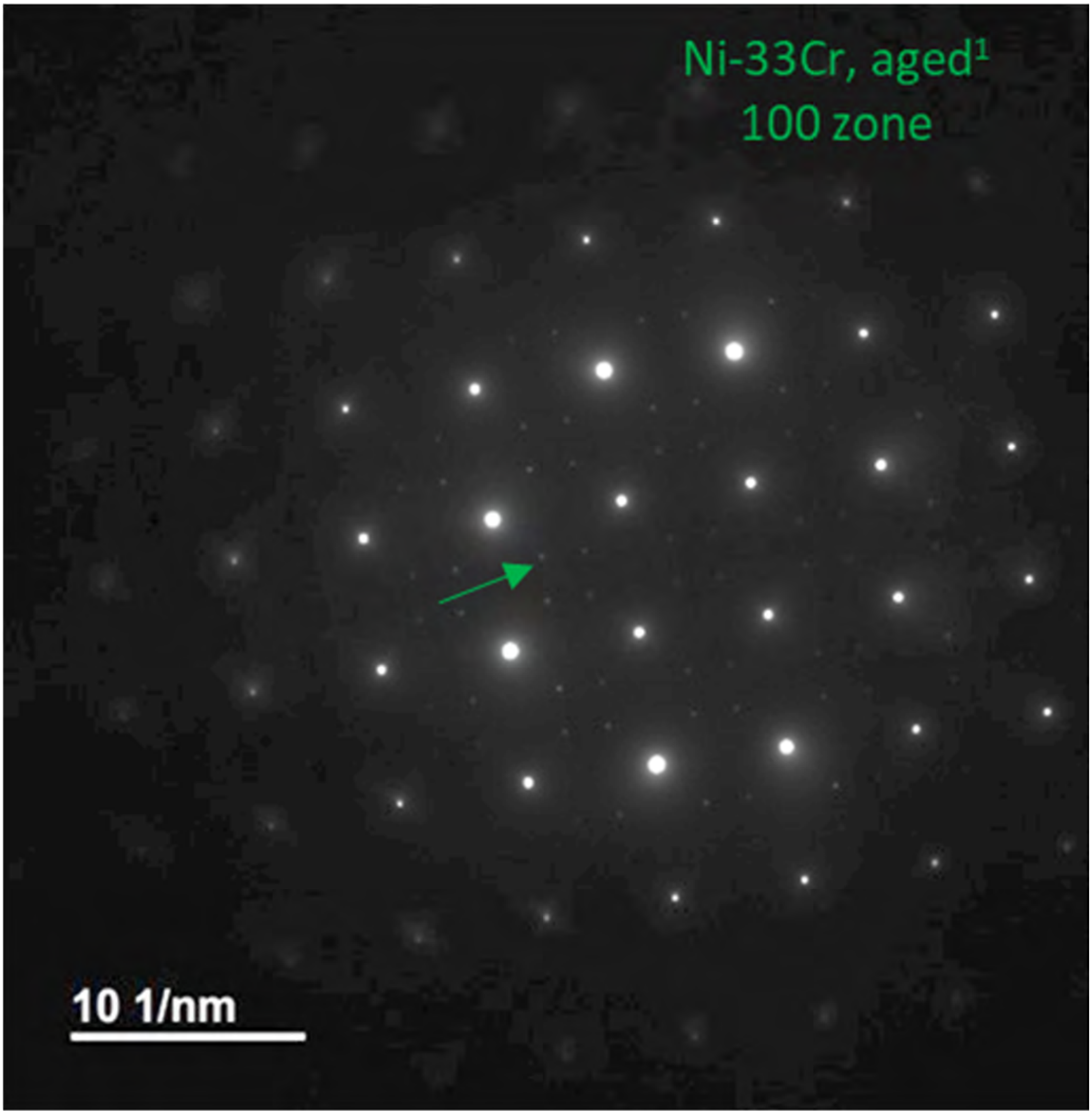

Figure 14 **Diffraction pattern from the model Ni-33C aged for at 475°C for 2,000h. The superlattice reflections (green arrow) confirm the presence of LRO.**

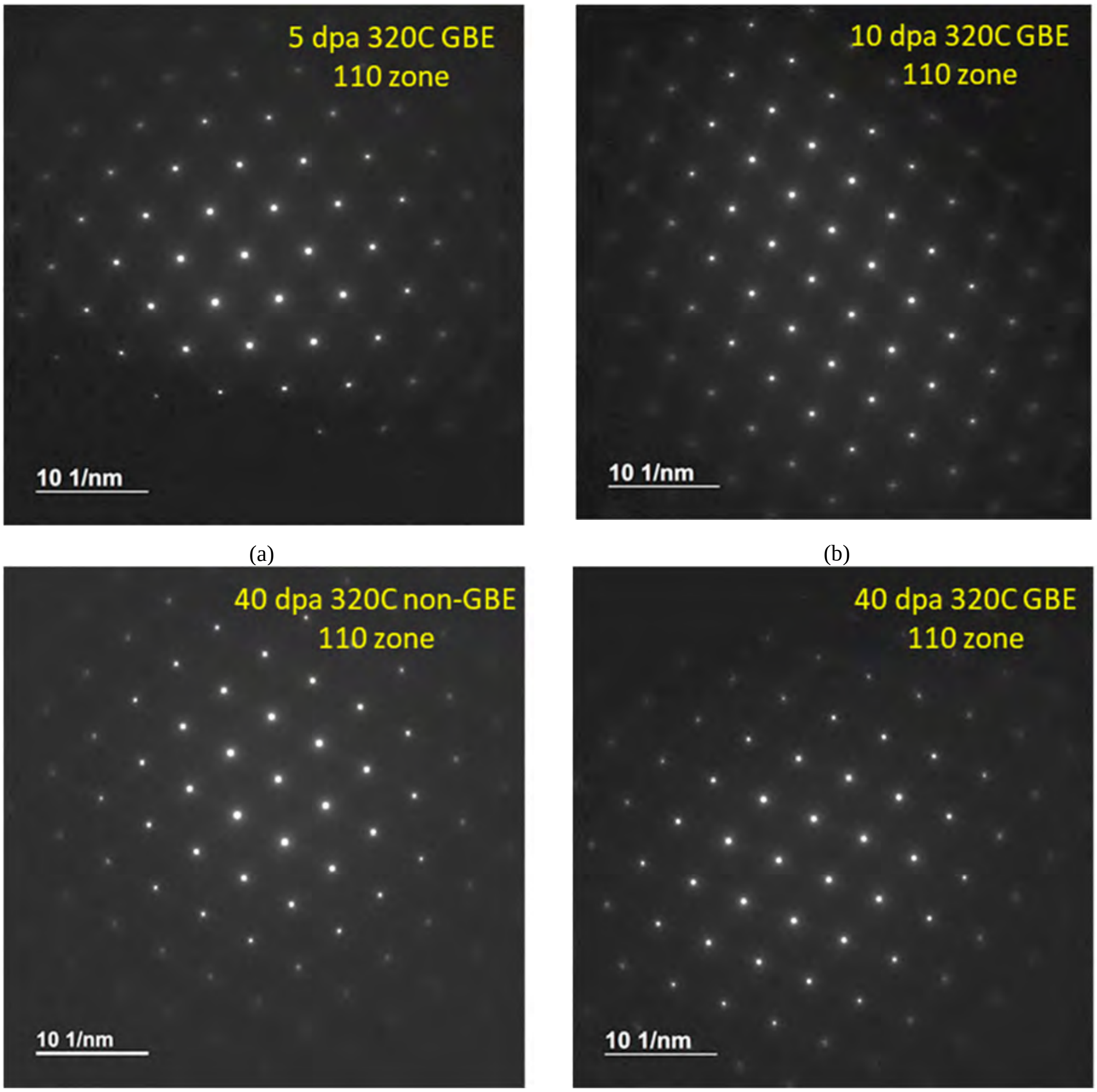

(a) (b)

(c) (d)

Figure 15 Diffraction patterns from Alloy 690 irradiated to (a) 5 dpa, (b) 10 dpa, and (c, d) 40 dpa. The absence of superlattice reflections suggest that LRO did not occur.

The TEM examination also focused on the occurrence and evolution of dislocation loops and voids. Figure 16 through Figure 19 show TEM images on the Alloy 690 neutron-irradiated specimens. Dislocation loops are the predominate features in the irradiated samples at all doses. A few precipitates (presumably $M_{23}C_6$ carbides) can also be seen occasionally. These carbides were present in unirradiated Alloy 690 as well, and thus not related to the neutron irradiation. Voids, in non-significant numbers, seem to occur only after the irradiation level has reached 40 dpa, as indicated with arrows in the figures.

Figure 20 shows the size distributions of dislocation loops at different irradiation levels. No significant difference exists among the irradiated samples, and the average size of dislocation loops were similar for different doses with or without prior GBE treatment. The loop density increased slightly with dose from

$1.7\text{x}10^{22}$ at 5 dpa to $2.5\text{x}10^{22}$ m^{-3} at 40 dpa. Nonetheless, the irradiated microstructure seems have been saturated above 5 dpa in Alloy 690 at PWR-relevant irradiation temperature.

Figure 21 shows a comparison of dislocation loop density at high angle grain boundaries (HAGB), small angle grain boundaries (SAGB), and twin boundaries (TB) as a function of irradiation level. The blue arrow shows precipitates at a SAGB. Preferential void or precipitate nucleation at GB or TB was NOT observed for all samples.

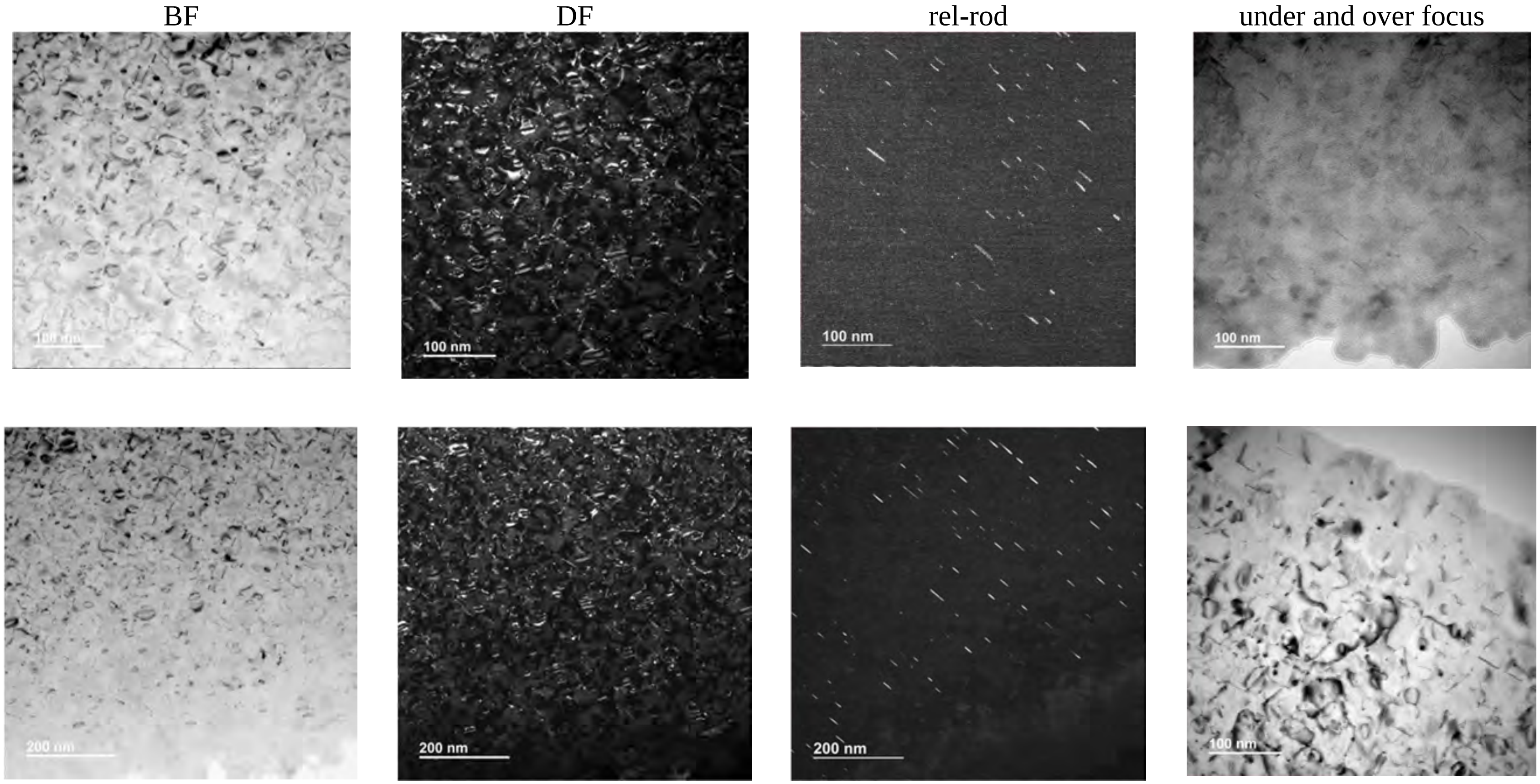

Figure 16 TEM images of loops and voids obtained on the 690GBE alloys irradiated to 5 dpa.

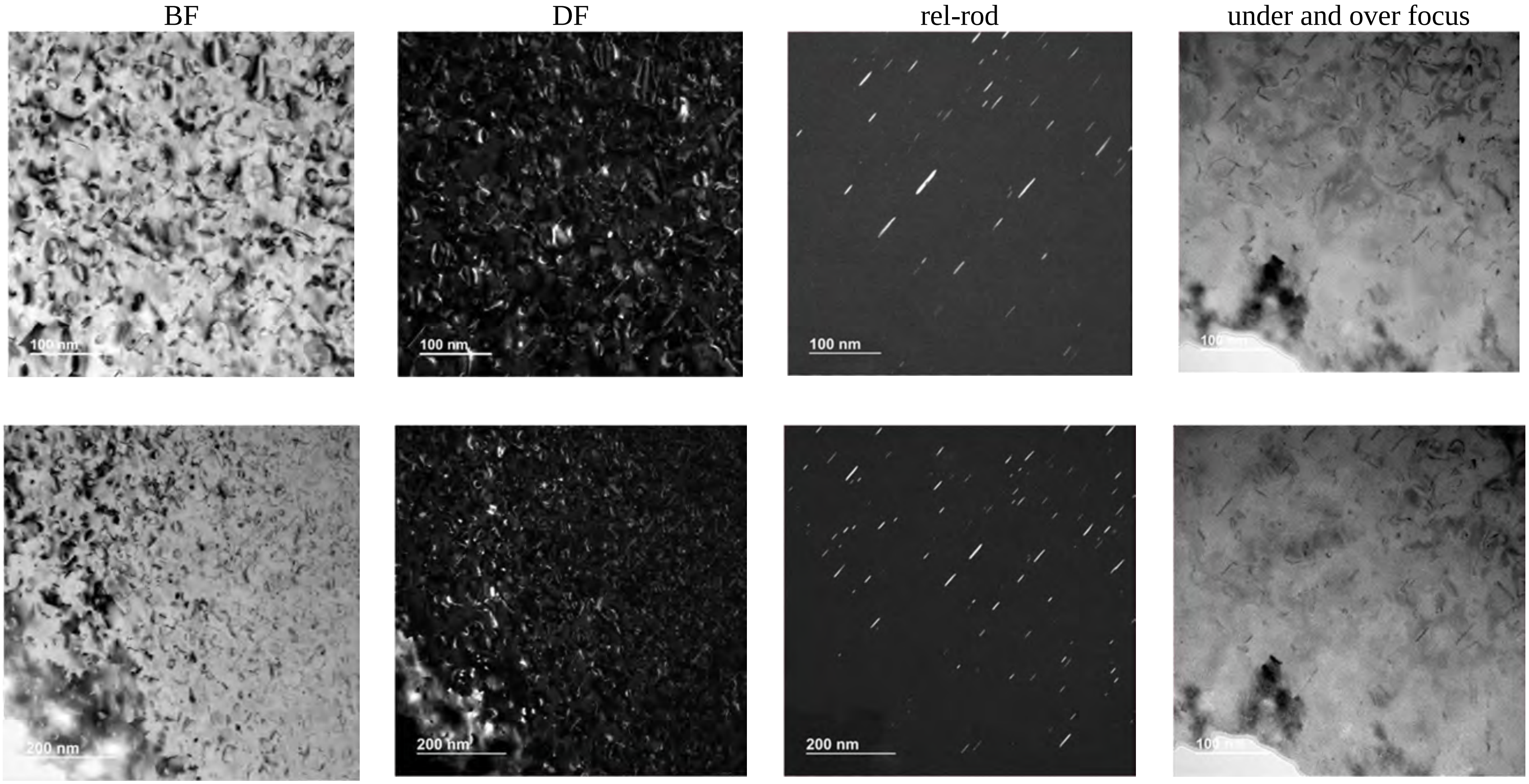

Figure 17 TEM images of loops and voids obtained on the 690GBE alloys irradiated to 10 dpa.

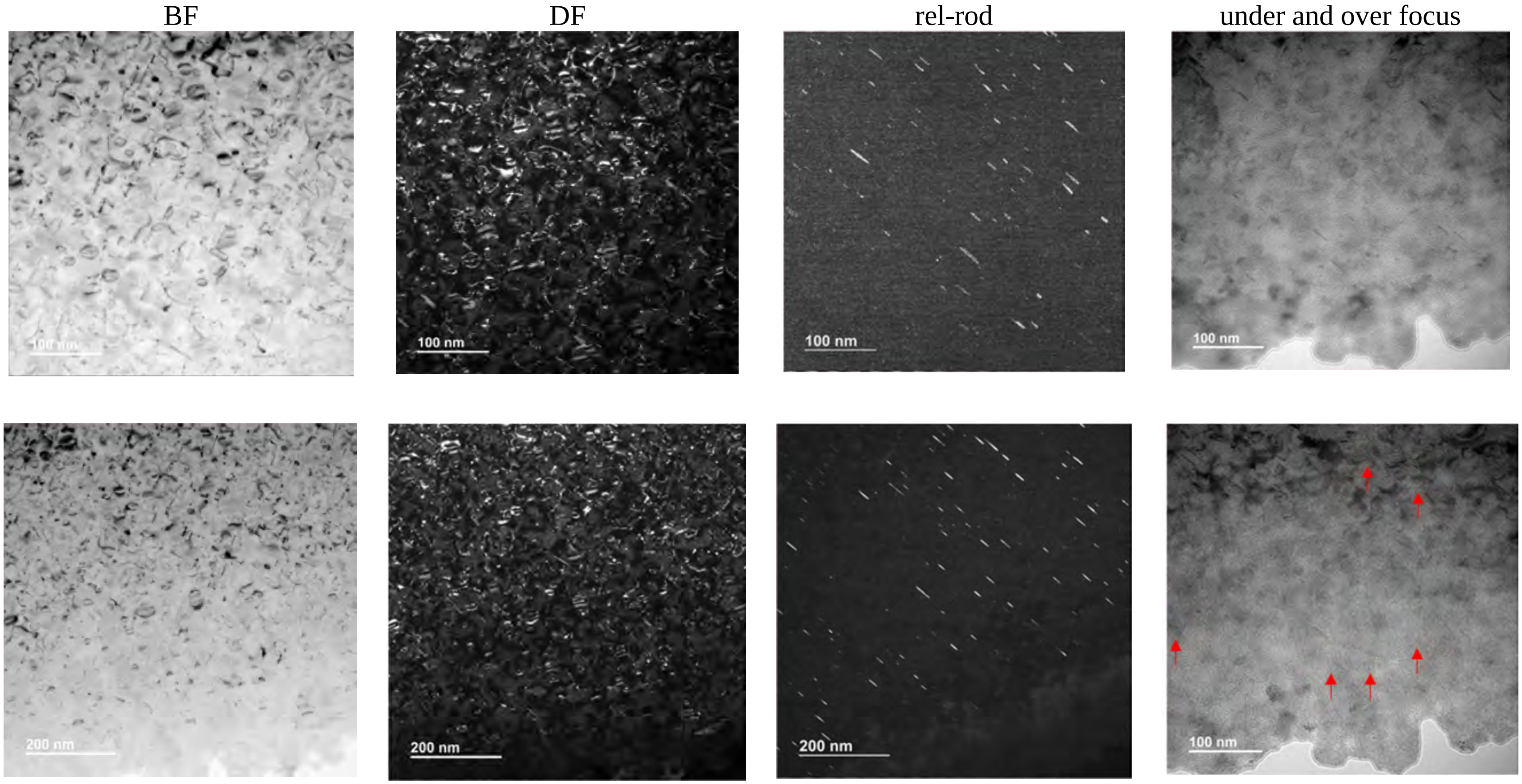

Figure 18 **TEM images of loops and voids obtained on the 690GBE alloys irradiated to 40 dpa. Red arrows indicate voids.**

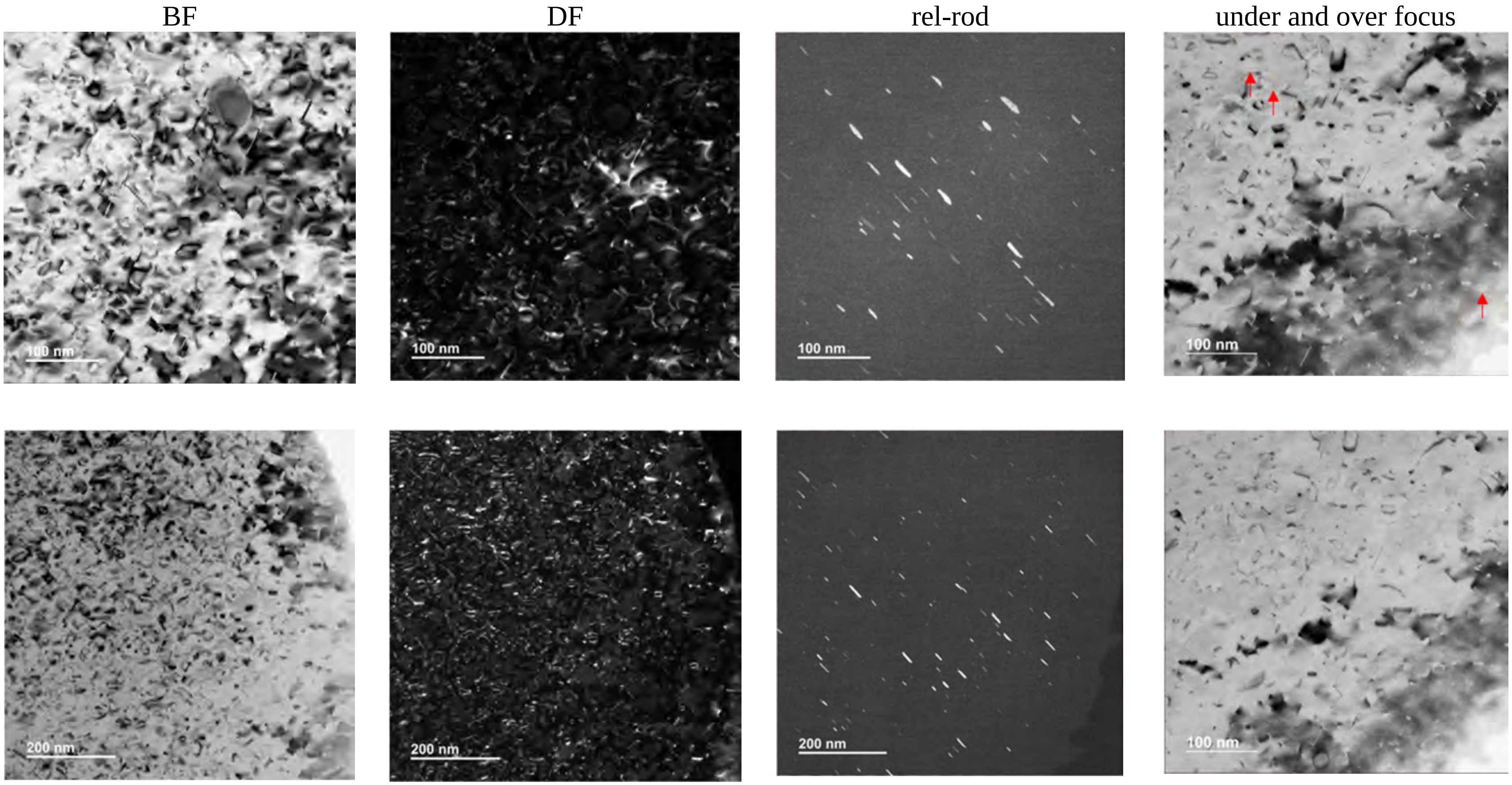

Figure 19 **TEM images of loops and voids obtained on the 690BASE alloys irradiated to 40 dpa. Red arrows indicate voids.**

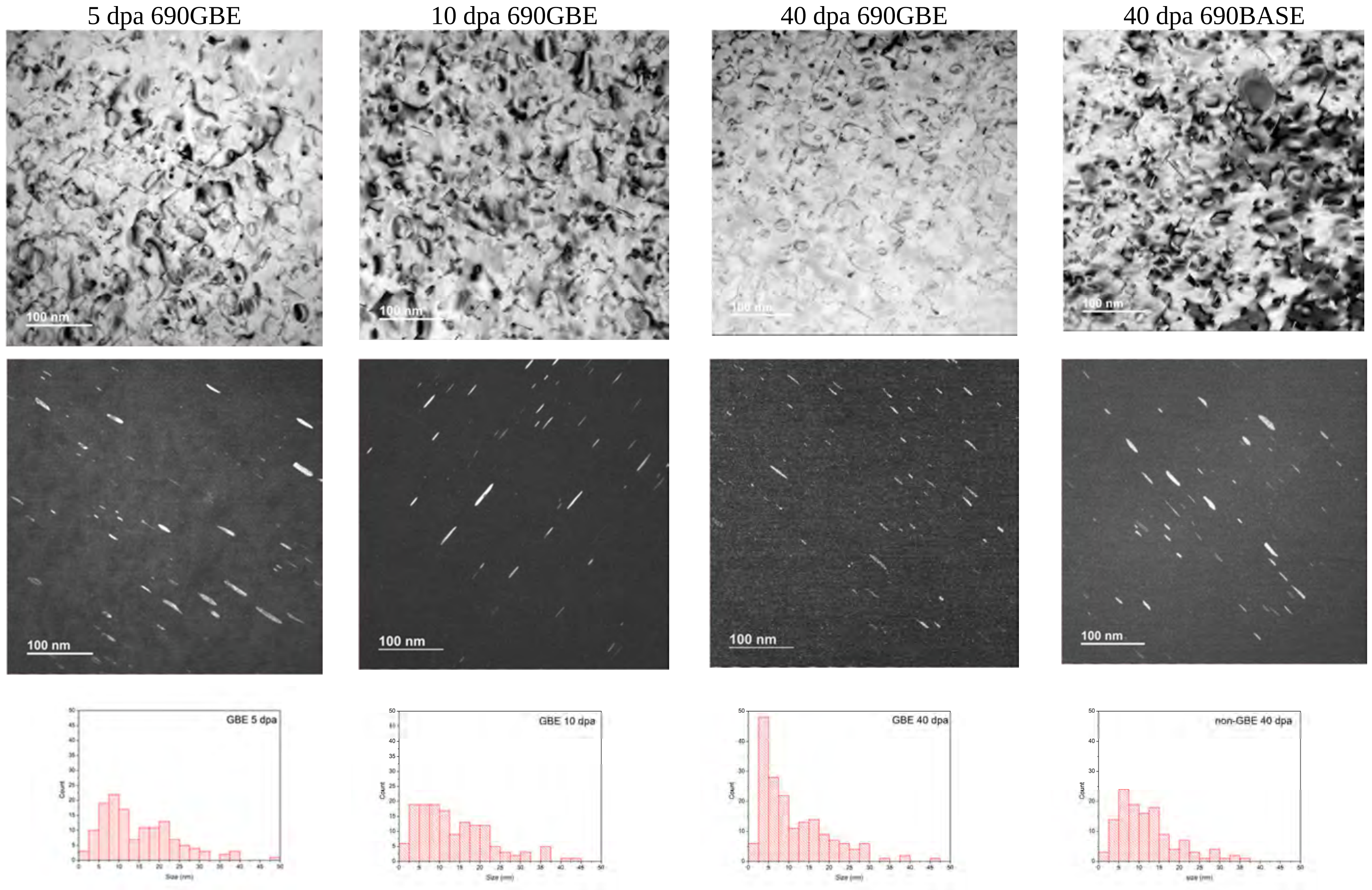

Size = 14.8 nm
Density = $1.7\text{x}10^{22}\ \text{m}^{-3}$

Size = 13.6 nm
Density = $1.5\text{x}10^{22}\ \text{m}^{-3}$

Size = 11.1 nm
Density = $2.2\text{x}10^{22}\ \text{m}^{-3}$

Size = 12.0 nm
Density = $2.5\text{x}10^{22}\ \text{m}^{-3}$

Figure 20 **Comparison of dislocation loop density as a function of irradiation level.**

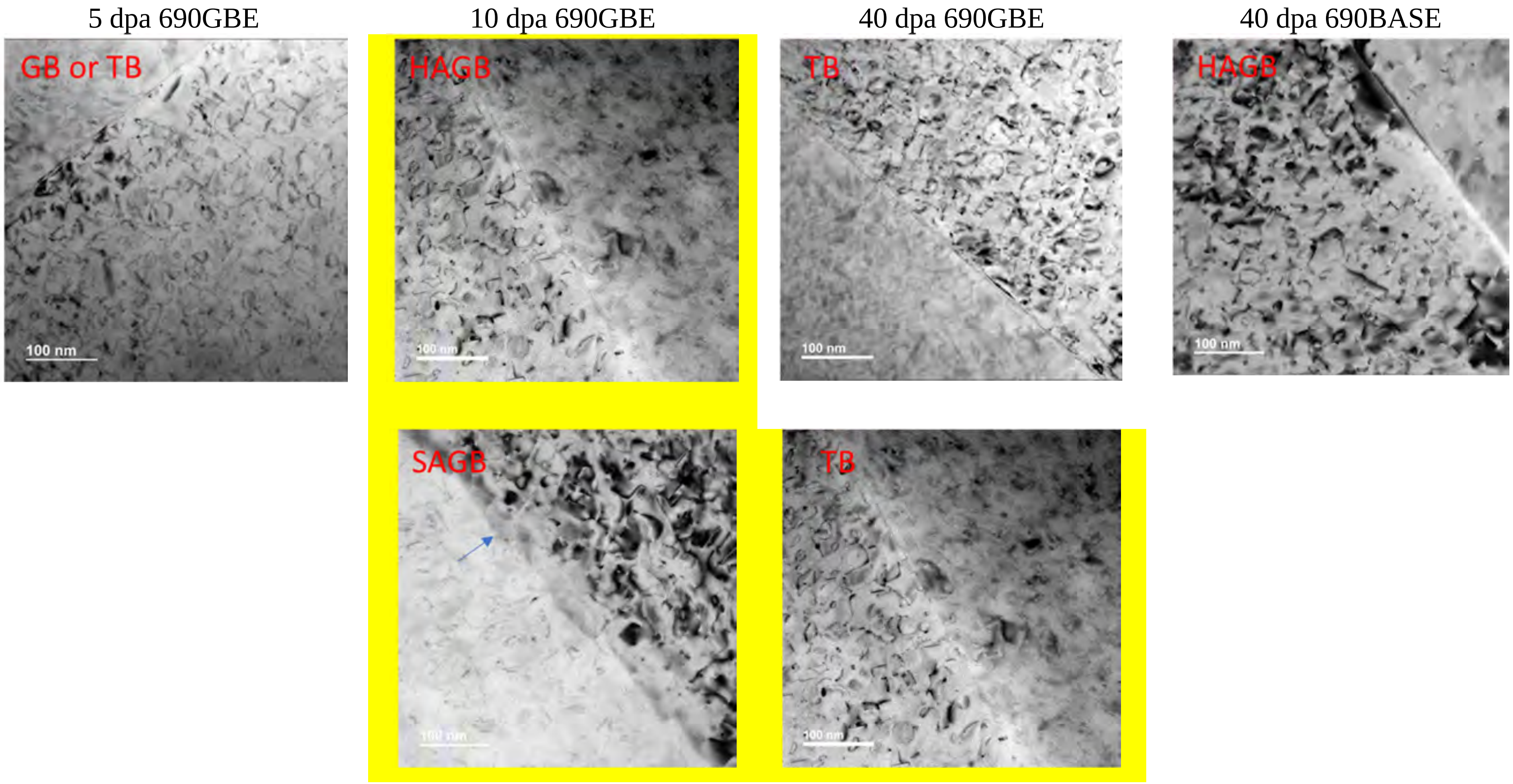

5 dpa 690GBE

10 dpa 690GBE

40 dpa 690GBE

40 dpa 690BASE

Figure 21 Comparison of dislocation loop density at high angle grain boundaries (HAGB), small angle grain boundaries (SAGB), and twin boundaries (TB) as a function of irradiation level. The blue arrow shows precipitates at a SAGB.

3.2 PWSCC Crack Growth Rate Testing

3.2.1 Crack growth rate testing of Alloy 690 Specimen 400-Y60, aged at 400°C for 29,445 h

The testing conditions for this specimen are given in Table 9, and the changes in crack length and K_{max} with time are shown in Figure 22. The test was initiated in simulated primary water at 320°C with in-situ precracking (Pre a – Pre e), and was followed by transitioning (test periods 1-5). The SCC CGR was evaluated under constant load in test period 6. The CGR response was low. Next, the crack was advanced in fatigue to a different microstructure, and the transitioning sequence was repeated. The SCC CGR was evaluated at the new location under constant load, and the response was again extremely low. Overall, the CGR response seems consistent with that of non-aged specimens.

Table 9 Crack growth data in PWR water[a] for Alloy 690 Specimen 400-Y60, aged at 400°C for 29,445 h.

Test Period	Test Time, h	Temp., °C	Load Ratio R	Rise Time, s	Down Time, s	Hold Time, s	K_{max}, MPa·m$^{1/2}$	ΔK, MPa·m$^{1/2}$	CGR_{env}, m/s	Estimated CGR_{air}, m/s	Crack Length, mm
Pre a	120	319.8	0.30	1	1	0	26.6	18.6	2.48E-08	3.48E-08	12.097
Pre b	138	319.6	0.30	50	50	0	26.7	18.7	5.94E-10	7.06E-10	12.136
Pre c	140	319.7	0.30	1	1	0	27.2	19.1	3.52E-08	3.82E-08	12.276
Pre d	142	319.5	0.30	2	2	0	27.5	19.3	2.44E-08	2.00E-08	12.365
Pre e	145	319.6	0.30	5	5	0	27.7	19.4	1.01E-08	8.19E-09	12.412
1	161	319.7	0.50	120	12	0	27.8	13.9	4.27E-10	1.51E-10	12.438
2	168	319.7	0.50	600	12	0	27.8	13.9	2.11E-10	3.00E-11	12.439
3	190	319.5	0.50	1000	12	0	27.8	13.9	4.90E-11	1.80E-11	12.447
4	281	319.6	0.50	1000	12	7,200	27.9	13.9	2.58E-11	2.21E-12	12.454
5	594	320.1	0.50	1000	12	14,400	27.9	14.0	2.03E-11	1.19E-12	12.470
6	919	320.8	1.00	0	0	0	27.9	0.0	no growth	-	12.470
7	921	320.0	0.30	1	1	0	28.5	20.0	6.13E-08	4.64E-08	12.618
8	936	320.3	0.30	50	50	0	28.8	20.1	2.16E-09	9.61E-10	12.686
9	938	320.3	0.30	1	1	0	29.6	20.7	7.01E-08	5.41E-08	12.894
10	944	320.7	0.50	120	12	0	29.6	14.8	6.70E-10	1.96E-10	12.919
11	985	320.2	0.50	600	12	0	29.8	14.9	1.70E-10	4.01E-11	12.941
12	1,057	320.3	0.50	1000	12	0	29.9	15.0	1.02E-10	2.44E-11	12.966
13	1,127	320.4	0.50	1000	12	7,200	30.0	15.0	2.50E-11	2.99E-12	12.973
14	1,156	320.4	0.50	1000	12	14,400	29.9	15.0	4.38E-12	1.58E-12	12.970
15	2,213	320.2	1.00	0	0	0	30.1	0.0	no growth	-	12.970

[a] Simulated PWR water with 2 ppm Li, 1000 ppm B, and 2 ppm H. DO<10 ppb. Conductivity is 21±3 μS/cm, and pH is 6.4.

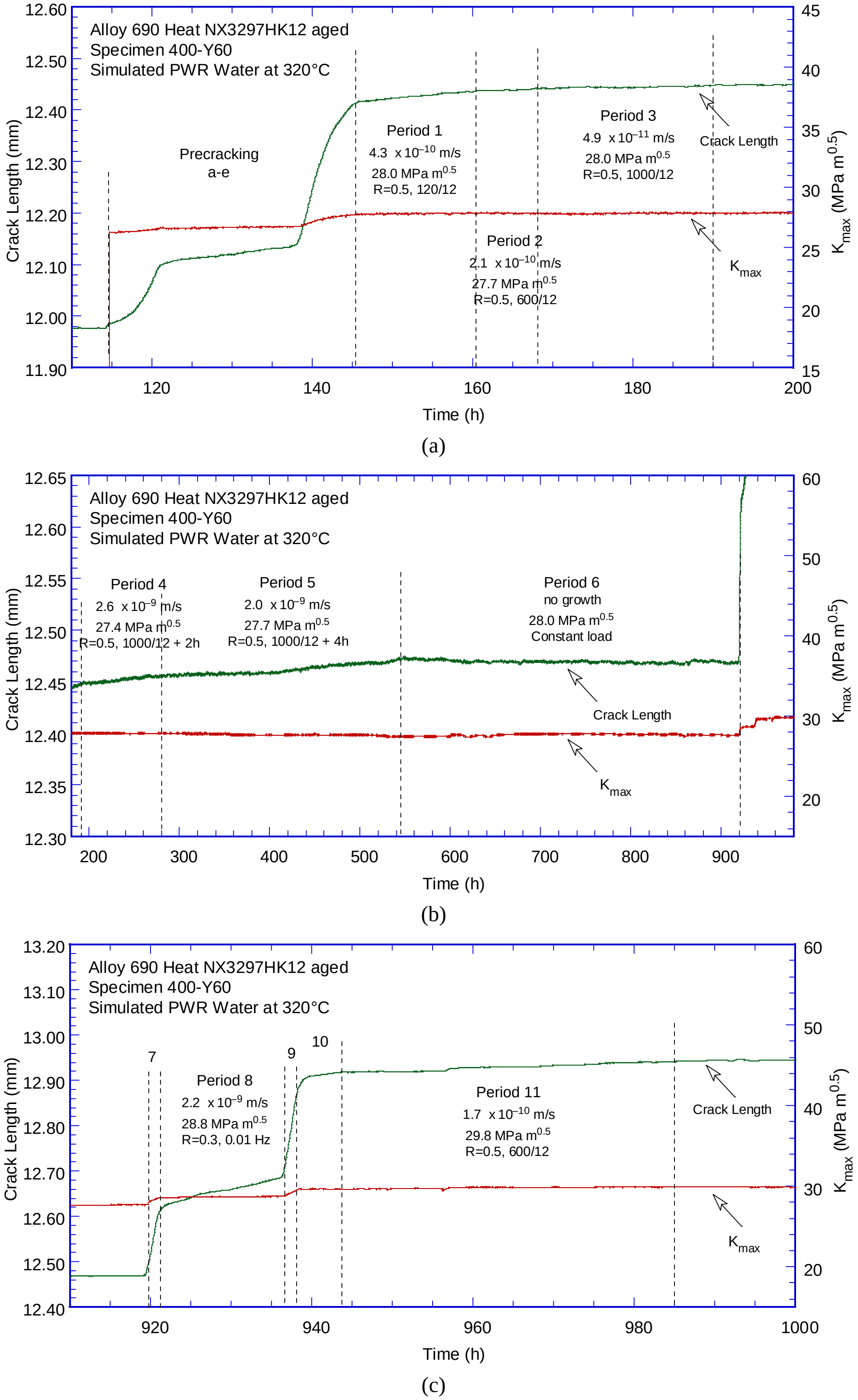

Figure 22 **Crack length vs. time in simulated PWR environment for Alloy 690 Specimen 400-Y60, aged at 400°C for 29,445h, during test periods: (a) precracking-3, (b) 4-6, (c) 7-11, and (d) 12-15.**

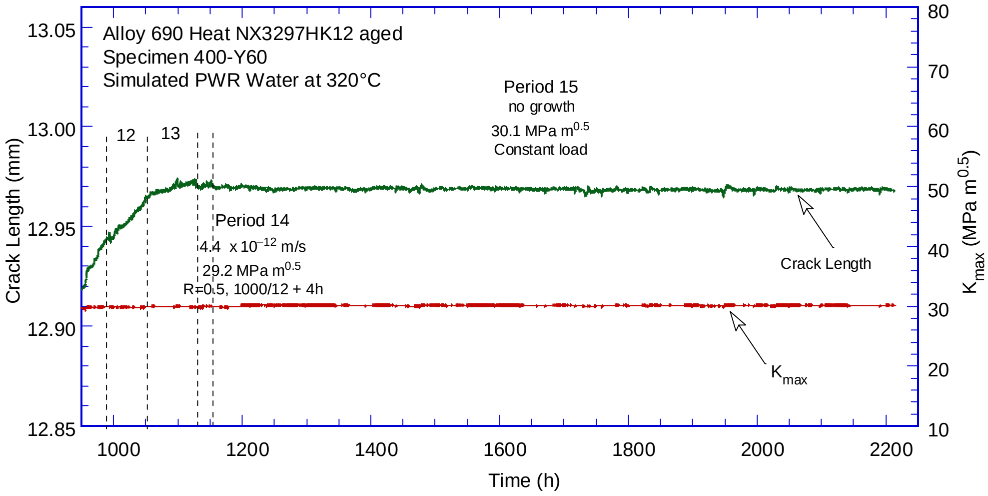

(d)

Figure 22 (cont.)

3.2.2 *Crack growth rate testing of Alloy 690 specimen 370-Y60, aged at 370°C for 74,808 h*

The testing conditions for this specimen are given in Table 10, and the changes in crack length and K_{max} with time are shown in Figure 23. The test was initiated with precracking in the 320°C water environment, and was followed by transitioning (test periods 1-4), and the first SCC CGR determination under constant load in test period 5. The response was low, so the crack was advanced to a new microstructure and the sequence was repeated. The second SCC CGR determination was made in test period 17. Upon reading a low SCC CGR value, an attempt was made to reactivate the crack by gentle cycling in test period 18, and this was followed by a final test period at constant load. The SCC CGR response in test period 19 was again low. As with the previous aged specimen, the overall CGR response, cyclic and SCC, seems to be consistent with that of non-aged specimens.

Table 10 Crack growth data in PWR water[a] for Alloy 690 Specimen 370-Y60 aged for 74,808 h at 370°C

Test Period	Test Time, h	Temp., °C	Load Ratio R	Rise Time, s	Down Time, s	Hold Time, s	K_{max}, MPa·m$^{1/2}$	ΔK, MPa·m$^{1/2}$	CGR_{env}, m/s	Estimated CGR_{air}, m/s	Crack Length, mm
Pre a	29	319.4	0.30	1	1	0	26.0	18.2	2.52E-08	3.17E-08	11.952
1	47	318.8	0.50	120	12	0	26.1	13.0	2.58E-10	1.14E-10	11.983
2	122	319.2	0.50	600	12	0	26.2	13.1	7.99E-11	2.35E-11	12.007
3	221	319.0	0.50	1000	12	0	26.3	13.2	4.72E-11	1.43E-11	12.024
4	365	318.5	0.50	1000	12	7,200	26.2	13.1	1.06E-11	1.71E-12	12.033
5	676	318.7	1.00	0	0	0	26.3	0.0	no growth	-	12.033
6	795	318.7	0.50	1000	12	7,200	26.4	13.2	9.17E-12	1.77E-12	12.045
7	797	319.6	0.30	1	1	0	26.6	18.6	3.30E-08	3.48E-08	12.127
8	818	319.9	0.30	50	50	0	26.9	18.8	1.49E-09	7.23E-10	12.185
9	797	319.6	0.30	1	1	0	27.5	19.2	4.52E-08	3.95E-08	12.362
10	821	319.4	0.50	120	12	0	27.5	13.8	4.34E-10	1.44E-10	12.398
11	843	319.6	0.50	600	12	0	27.7	13.8	1.56E-10	2.95E-11	12.409
12	867	319.9	0.50	1000	12	0	27.5	13.8	8.59E-11	1.73E-11	12.416
13	892	319.4	0.50	1000	12	7,200	27.6	13.8	2.41E-11	2.13E-12	12.420
14	1,321	319.5	1.00	0	0	0	27.8	0.0	2.14E-12	-	12.423

Table 10 (cont.)

Test Period	Test Time, h	Temp., °C	Load Ratio R	Rise Time, s	Down Time, s	Hold Time, s	K_{max}, MPa·m$^{1/2}$	ΔK, MPa·m$^{1/2}$	CGR_{env}, m/s	Estimated CGR_{air}, m/s	Crack Length, mm
15	1,606	319.8	0.50	1000	12	0	27.7	13.9	8.01E-11	1.77E-11	12.515
16	1,750	319.0	0.50	1000	12	7,200	28.2	14.1	1.66E-11	2.32E-12	12.526
17	2,898	319.4	1.00	0	0	0	28.2	0.0	1.38E-12	-	12.527
18	3,037	319.5	0.50	1000	12	7,200	28.1	14.0	1.62E-11	2.27E-12	12.536
19	4,243	319.5	1.00	0	0	0	28.2	0.0	6.98E-13	-	12.539

[a] Simulated PWR water with 2 ppm Li, 1000 ppm B, and 2 ppm H. DO<10 ppb. Conductivity is 21±3 µS/cm, and pH is 6.4.

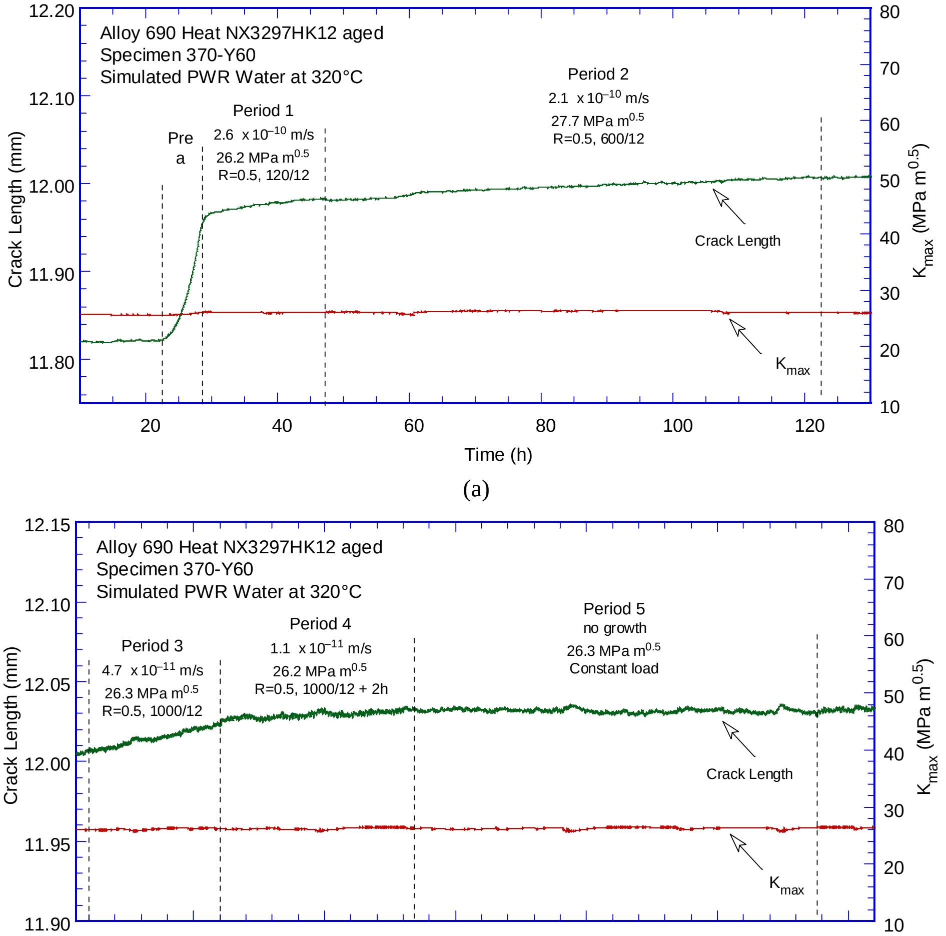

Figure 23 **Crack length vs. time in simulated PWR environment for Alloy 690 Specimen 370-Y60, aged for 74,808 h at 370°C, during test periods: (a) precracking-2, (b) 3-5, (c) 6-13, (d) 14-17, and (e) 18-19.**

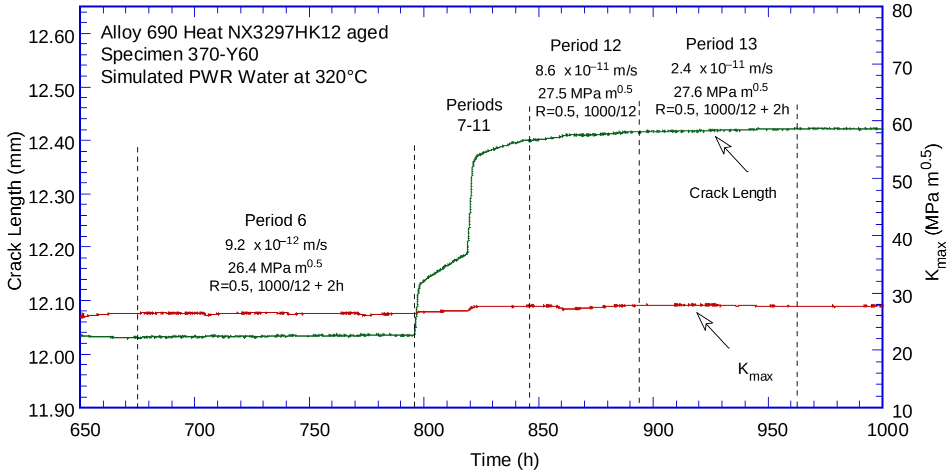

(c)

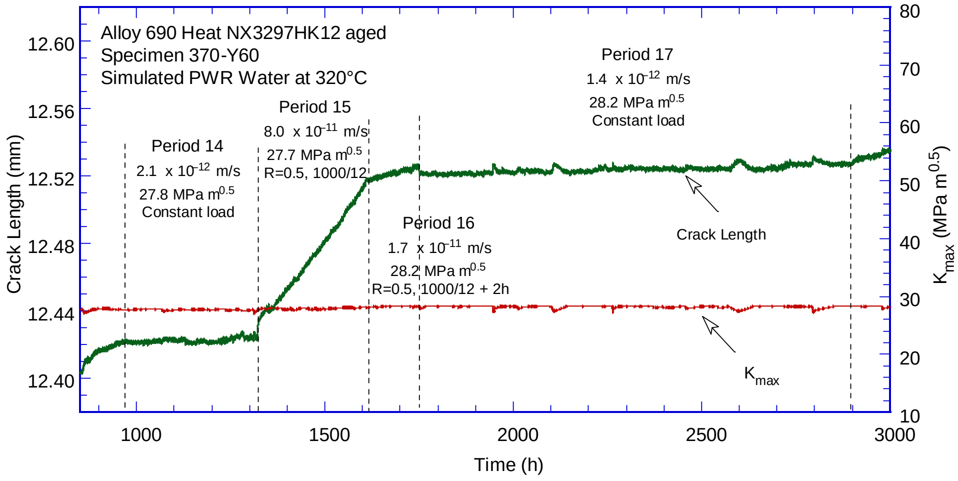

(d)

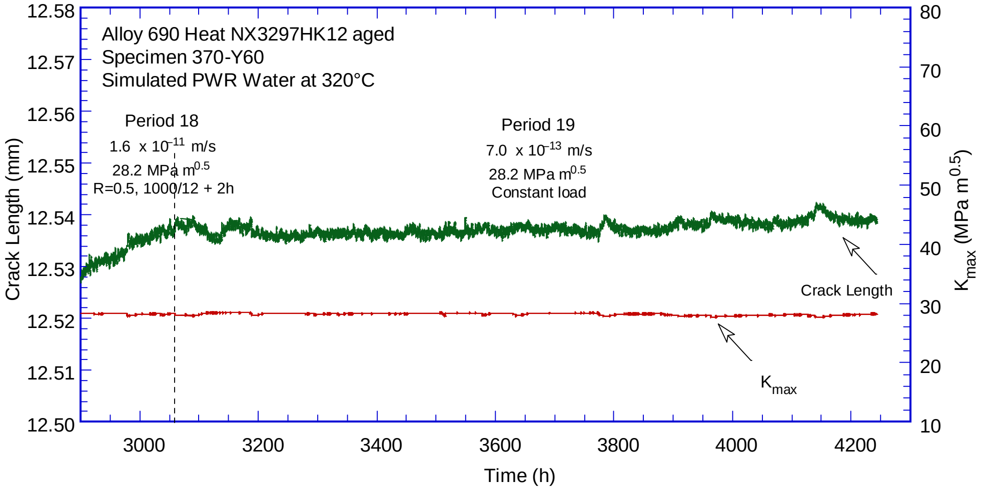

(e)

Figure 23 (cont.)

4 Discussion

This section provides summary of the aging and irradiation effects in Alloy 690 and discusses the potential implications on performance. The testing results of aged alloys are discussed in the framework provided by the well-established fatigue and corrosion fatigue behavior for these alloys, as well as the industry-proposed disposition curves for crack growth.

4.1 Effects of aging and neutron-irradiation on microstructure of Alloy 690

4.1.1 Hardness

The hardness of aged Alloy 690 specimens, irrespective of aging temperature – 370°C, 400°C, or 450°C – was found to increase with aging time, Figure 11. The increases are similar, except for 370-Y30, where hardness appears to decrease with additional aging. Coincidentally similar to the study by Houtilainen [37] mentioned previously, 400°C was one of the aging temperatures in the ANL effort as well, however, the aging times of 13,000 and 29,000 h in the ANL study were significantly longer than those in reference [37]. It is also interesting to note that similar to the heats in reference [37], the Fe content in the ANL heat is also less than 10 wt. % (9.9 and 8.53 wt. % in two independent measurements, Table 1). However, the resulting hardening in the ANL heat ($\Delta H \cong 30$) is less than that reported by Houtilainen ($\Delta H \cong 40$-100, [37]), but closer to that reported by Young [3]. The hardening in the latter study was demonstrated to be due to LRO.

While LRO and its effect on SCC response is one of the main questions that this research is attempting to answer, it is important to keep in mind that the microstructural effects of thermal aging have been studied extensively in the past, leading to a comprehensive understanding of thermally-induced Cr carbide precipitation along grain boundaries [24], further resulting into an overall an increase in hardness. From an SCC susceptibility standpoint, Cr carbide precipitation depletes Cr from solution, and thus could potentially decrease resistance to SCC. In essence, an increase in hardness, whether due to LRO formation or Cr-carbide precipitation, or both, can potentially have only a negative effect on the SCC resistance, and hence needs to be investigated experimentally. The two tests presented in this report address that need.

4.1.2 Long range Ordering (LRO) in Alloy 690 aged or neutron-irradiated

LRO was not detected in the aged or the neutron irradiated specimens. It is significant to note that the Alloy 690 Heat NX3297HK12 used in the aging study has a Fe content below 10 wt. % (9.9 and 8.53 wt. % in two independent measurements, Table 1), so it could have been be prone to developing LRO under long term exposure. For the neutron-irradiated alloys, one heat, 690 GBE, has a Fe content of 10.26 wt. % which makes it comparable to that used in [8], in which proton irradiation of 2.5 dpa at 360°C was found induce LRO. The Fe level in the second neutron-irradiated Alloy 690 heat, 690 BASE, was 9.02 wt. %, so it would have been be prone to LRO formation.

4.1.3 Microstructure of Neutron-Irradiated Alloy 690

No LRO was detected among the neutron-irradiated Alloy 690 as evident by the lack of superlattice reflections in the zone axes. This result contradicts to the proton-irradiation study where LRO was clearly visible at ~2 dpa. One possible reason for this discrepancy is the irradiation temperature. While the proton irradiation was performed at 360C, the BOR-60 irradiation was conducted at a lower temperature. Additional investigation is needed to explore a wider range of irradiation temperature and dose rate.

Dislocation loops were the dominate microstructure in the Alloy 690 irradiated at PWR-relevant temperature. With the increasing dose from 5 to 40 dpa, the dislocation density increased slightly while the dislocation size remained the same. Scattered carbides can be seen in unirradiated 690, and neutron irradiation did not change the pre-exist carbides. Although small voids of a few nm in size were observed at 40 dpa, their density was extremely low. As a result, volumetric swelling resulting from these voids would be negligibly small for these samples. This is consistent with previous study on austenitic stainless steels that, void formation is insignificant for irradiations at PWR-relevant temperature.

The TEM characterization also revealed that the GBE treatment did not lead to significantly different irradiation microstructure. The evolution of the dislocation loops was similar near high-angle and CSL boundaries in Alloy 690, and no difference was detectable up to 40 dpa.

4.2 Effects of aging on crack growth response of Alloy 690

4.2.1 Cyclic response of aged Alloy 690

Figure 24 presents the cyclic CGR data obtained on Alloy 690 Heat NX3297HK12 in the as-received and two aged conditions. In the figure, the cyclic CGRs measured in the environment are plotted vs. the CGRs predicted in air under the same loading conditions for Alloy 690. In this representation, the environmental enhancement, i.e., the departure from the “1:1 diagonal” can be easily visualized. Correlations describing cyclic CGRs in air and LWR environments have been established by ANL for Alloy 600, 690, Ni-base weldments as well as SSs [25-29]. For comparison, the expected cyclic CGR curve for Alloy 600 was also included. Figure 24 shows that, as expected, the cyclic CGRs in the mechanical fatigue regime (10^{-8}-10^{-7} m/s) are exactly as expected, and that is true for both aged specimens as well as the specimen tested in the un-aged, as-received (AR) condition. In fact, it is the un-aged specimen whose fatigue CGRs are slightly lower than expected, and that may be due to the fact that this specimen was purposely aligned in a region with a high density of Cr-carbide and grain size banding as, at the time, these microstructural features were believed to promote SCC [14]. In the corrosion fatigue regime (10^{-11}-10^{-9} m/s), there is no difference between the aged specimens and the non-aged, AR specimen. Also, unsurprisingly, at the lower end of the spectrum, the environmental enhancement of all three Alloy 690 specimens is lower than the Alloy 600 curve.

In summary, the fatigue and corrosion fatigue CGR response of the two Alloy 690 Heat NX3297HK12 specimens aged to 60-year service equivalents is similar to that of the un-aged condition.

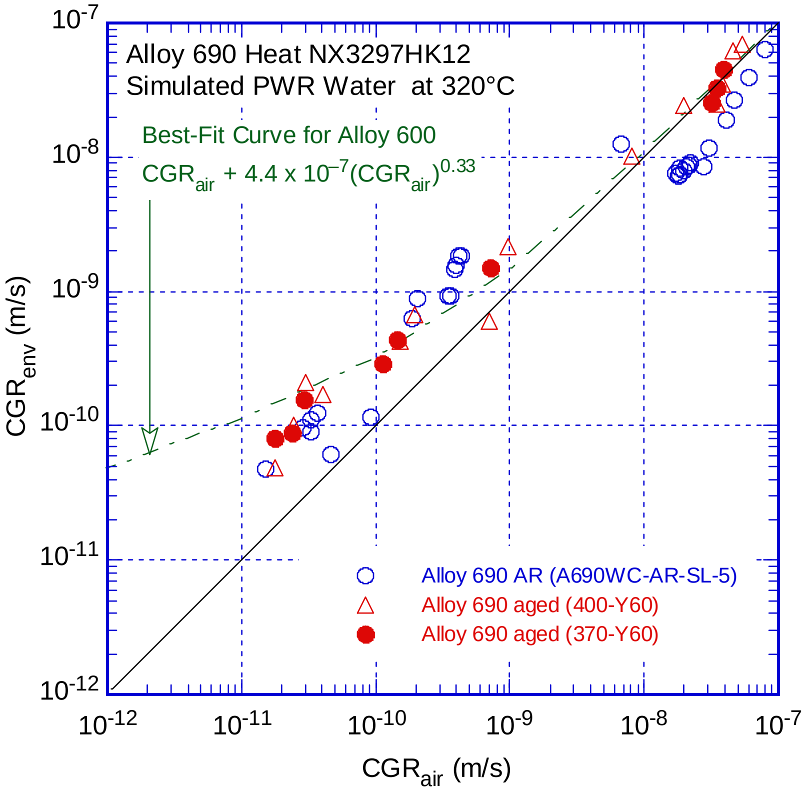

Figure 24 **Cyclic CGRs measured in the environment vs. CGRs predicted in air under the same loading conditions for Alloy 690 Heat NX3297HK12 in the as-received and two aged conditions.**

4.2.2 SCC response of aged Alloy 690

Figure 25 presents the SCC CGR data for the Alloy 690 Heat NX3297HK12 in the as-received and two aged conditions vs. stress intensity factor, K. For context, the proposed disposition curves for Alloys 600 [30] and 690 [2] are included. The “no growth” SCC CGRs are plotted at 1×10^{-13} m/s as proposed in ref. [1]. Figure 25 shows that the SCC CGR data for the un-aged, AR specimen was “no growth” despite increasing K to over 50 Mpa $m^{1/2}$. Likewise, the SCC CGR data for the aged specimen was either “no growth” or extremely small. The EPRI MRP-386 [2] proposed disposition curve seems to bound the SCC CGR data from both the aged and un-aged specimens, hence, aging to 60-year service equivalents did not have a negative effect on the SCC resistance of this Alloy 690 heat.

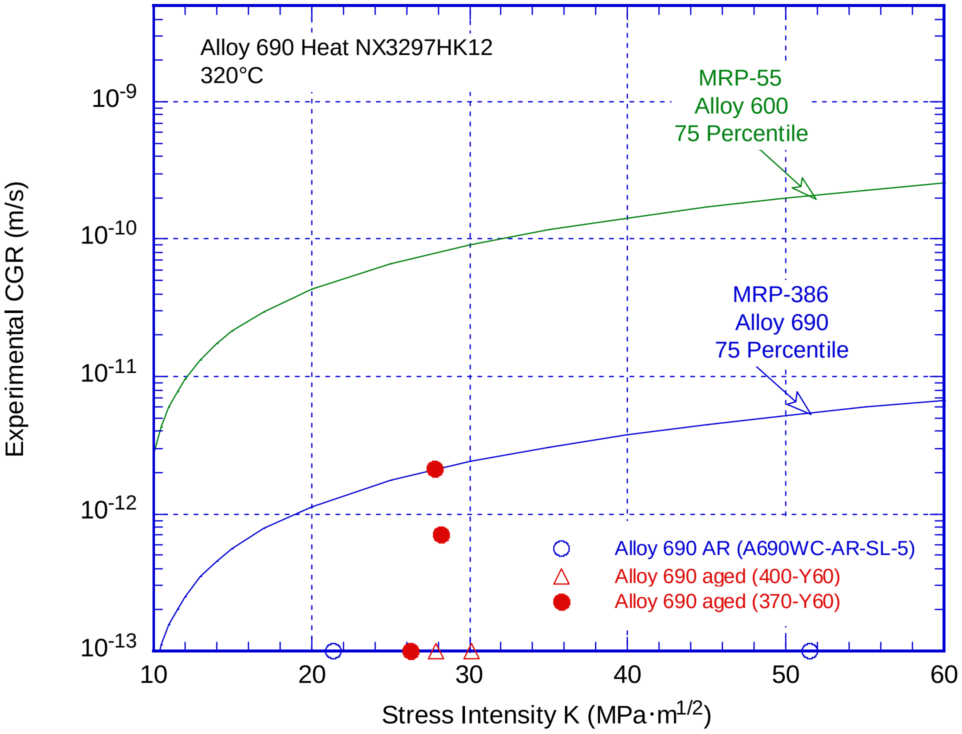

Figure 25 SCC CGRs for Alloy 690 Heat NX3297HK12 in the as-received (AR) and aged conditions. The data obtained on the as-received specimen was included in the MRP-386 [2] database (ID 501-502) and were used in the determination of the proposed disposition curve for Alloy 690 [2]. The proposed disposition curves for Alloys 690 [2] and 600 [30] are also included for comparison.

5 Conclusions

The need for an assessment of the long term aging effects on performance in Alloy 690 and associated weldments was identified as a research gap in the Light Water Reactor Sustainability (LWRS) stakeholders report for 2020 [9], being recognized as such by both industry [2, 10] and regulators [11]. The research undertaken in this program is beginning to address that gap. Specifically, the work focused on the microstructural evolution and the SCC response of Alloy 690 under accelerated thermal aging and irradiation conditions. The materials studied involved Alloy 690 from two sources: (i) Alloy 690 plate from an Alloy 152 dissimilar metal weld (DMW) joining the Alloy 690 plate and Alloy 533, aged at three different temperatures (370°C, 400°C and 450°C) for up to 75,000h, and (ii) specimens neutron-irradiated in the BOR-60 reactor up to 40 dpa. The conclusions of the program are as follows:

- For aged Alloy 690 specimens, hardness was found to increase with aging time, however, the microstructural characterization by means of synchrotron X-ray did not find evidence of LRO.
- The microstructural characterization of neutron-irradiated Alloy 690 specimens by TEM found no evidence of LRO.
- Dislocation loops were the dominant defects in the neutron-irradiated Alloy 690. Preexisting carbide precipitates were not affected by the irradiation, and void swelling was negligible at 40 dpa.
- Testing in a primary water environment of Alloy 690 specimens aged to a 60-year service equivalent revealed a fatigue and corrosion fatigue crack growth responses similar to those measured on the un-aged alloy. The SCC CGR response was also low, with individual data points bound by the SCC disposition curve proposed in EPRI MRP-386 [2].
- Overall, the Alloy 690 heats aged up to 60-year service equivalents of exposed to neutron irradiation up to 40 dpa did not exhibit a deterioration in microstructure or performance.

References

1. Materials Reliability Program: Crack Growth Rates for Evaluating Primary Water Stress Corrosion Cracking (PWSCC) of Alloy 82, 182, and 132 Welds (MRP-115), EPRI, Palo Alto, CA: 2004. 1006696.
2. Electric Power Research Institute, "Recommended Factors of Improvement for Evaluating Primary Water Stress Corrosion Cracking (PWSCC) Growth Rates of Thick-Wall Alloy 690 Materials and Alloy 52, 152, and Variants Welds (MRP-386)," Palo Alto, CA, 2017: 3002010756.
3. Young, G.A., Morton, D.S., Lewis, N. Morris, R., Pyle, J., Barnard, L., Najafabadi, R., Effect of Long Range Order on the Stress Corrosion Susceptibility of a Nickel-33 at% Chromium Alloy, Corrosion 72 2016 1433.
4. Marucco, A., Atomic Ordering in the Ni-Cr-Fe system, Mat. Sci. and Eng. A189 (1994) 267.
5. F. Delabrouille, D. Renaud, F. Vaillant, J. Massoud, Long range ordering of Alloy 690, in: 14th. Int. Conf. On Environmental Degradation of Materials in Nuclear Power Systems, 2009, pp. 888-894.
6. Brimbal, D., Joly, P., Benhamou, C., Thermal aging of Ni-Cr and Ni-Cr-Fe alloys to determine the potential for long-range ordering of Alloy 690 at PWR relevant temperatures, EPRI PWSCC Research Collaboration Meeting 2019, Tampa, Florida, December 4th, 2019.
7. Houtilainen, C., Ehrnstén, U., Ahonen, M., Hänninen, H., Effect of Thermal Aging on Microstructure and Hardness of Industrial Heats of Alloy 690, 19th. Int. Conf. On Environmental Degradation of Materials in Nuclear Power Systems, 2019.
8. Song, M., Yang, Y., Wang, M., Kuang, W., Lear, C.L., Was, G.S., Probing long-range ordering in nickel-base alloys with proton Irradiation, Acta Materialia 156 (2018) 446-462.
9. Light Water Reactor Sustainability Program Stakeholder Engagement Meeting Summary Report, INL/EXT-19-54520, February, 2020.
10. Burke, M., Coordination of EPRI Issue Programs' Research Activities with LWRS Materials Pathway Projects, LWRS Materials Research Pathway Stakeholder Engagement Meetings, August 18, 2020.
11. Collins, J., and Focht, E., Nickel-Based Alloy Crack Growth Rates, Industry / NRC Materials Programs Technical Information Exchange, August 11, 2021, ML21217A260.
12. Material Documentation Report for Consumers Power Midland (620-0012-51) and TMI-2 (620-0006-51) Reactor Vessel Lower Head Material, The Babcock & Wilcox Company, BAW-2071, January 1989.
13. Dunn, D., Alexandreanu, B., Toter, W., "Shielded Metal Arc Welding Parameters for Primary Water Stress Corrosion Cracking Test Materials," Technical Letter Report ML13171A113, June 2013.
14. Alexandreanu, B., Y. Yang, Y. Chen, and W. J. Shack, "Stress Corrosion Cracking in Nickel-Base Alloys 690 and 152 Weld in Simulated PWR Environment - 2009," NUREG/CR–7137, ANL–10/36, June 2012.
15. Alexandreanu, B., Chen, Y., Natesan, K., and Shack, "Primary Water Stress Corrosion Cracking of High-Chromium, Nickel-Base Welds Near Dissimilar Metal Weld Interfaces," NUREG/CR–7226, ANL–16/10, January 2018.
16. Alexandreanu, B., Chen, Y., Natesan, K., and Shack, "Primary Water Stress Corrosion Cracking of High-Chromium, Nickel-Base Welds - 2018," NUREG/CR–7276, 2021.
17. Choi, K.J., Kim, J.J, Bong, H.L., Bahn, C.B., Kim, J.H., Effects of thermal aging on microstructures of low alloy steel–Ni basealloy dissimilar metal weld interfaces, Journal of Nuclear Materials 441 (2013) 493-502.

18. Yoo, S.C., Choi, K.J., Bahn, C.B., Kim, S.H., Kim, J.Y., Kim, J.H., Effects of thermal aging on the microstructure of Type-II boundaries in dissimilar metal weld joints, Journal of Nuclear Materials 459 (2015) 5-12.
19. B. Alexandreanu, B. Capell and G.S. Was, Combined Effect of Special Grain Boundaries and Grain Boundary Carbides on IGSCC of Ni-16Cr-9Fe-xC Alloys, *Mat. Sci. and Eng.* A 300 (2001) 94.
20. Gwalani, B., Alam, T., Miller, C., Rojhirunsakool, T., Kim, Y.S., Kim, S.S., Kaufman, M., Ren, Y., and Banerjee, R., (2016). Experimental investigation of the ordering pathway in a Ni-33 at.%Cr alloy. Acta Materialia. 115. 372-384. 10.1016/j.actamat.2016.06.014.
21. American Society for Testing and Materials, “Standard Test Method for Measurement of Fatigue Crack Growth Rates,” ASTM E647-08, DOI 10.1520/E0647-08, West Conshohocken, PA, 2008.
22. American Society for Testing and Materials, “Standard Test Method for Determining a Threshold Stress Intensity Factor for Environment-Assisted Cracking of Metallic Materials,” ASTM E1681-03, DOI 10.1520/E1681-03R08, West Conshohocken, PA, 2008.
23. Electric Power Research Institute, “PWR Primary Water Chemistry Guidelines,” Volume 1, Revision 4, EPRI, Palo Alto, CA, 1999.
24. Angeliu, T.M., and Was, G.S., Behavior of grain boundary chemistry and precipitates upon thermal treatment of controlled purity Alloy 690, Metall. Trans. A 21A, 2097 (1990).
25. Ruther, W. E., W. K. Soppet, and T. F. Kassner, “Corrosion Fatigue of Alloys 600 and 690 in Simulated LWR Environments,” NUREG/CR-6383, ANL-95/37, April 1996.
26. Ruther, W. E., W. K. Soppet, T. F. Kassner, and W. J. Shack, “Environmentally Assisted Cracking of Alloys 600 and 690 in Simulated LWR Water,” in Environmentally Assisted Cracking in Light Water Reactors, Semiannual Report, January 1998-July 1998, NUREG/CR-4667, Vol. 26, ANL-98/30, pp. 25-32, March 1999.
27. Chopra, O. K., W. K. Soppet, and W. J. Shack, “Effects of Alloy Chemistry, Cold Work, and Water Chemistry on Corrosion Fatigue and Stress Corrosion Cracking of Nickel Alloys and Welds,” NUREG/CR-6721, ANL-01/07, April 2001.
28. Alexandreanu, B., O. K. Chopra, and W. J. Shack, “Crack Growth Rates of Nickel Alloys from the Davis-Besse and V. C. Summer Power Plants in a PWR Environment,” NUREG/CR–6921, ANL–05/55, November 2006.
29. Alexandreanu, B., O. K. Chopra, and W. J. Shack, “Crack Growth Rates of Nickel Alloy Welds in a PWR Environment,” NUREG/CR–6907, ANL–04/3, May 2006.
30. Electric Power Research Institute, “Materials Reliability Program (MRP) Crack Growth Rates for Evaluating Primary Water Stress Corrosion Cracking (PWSCC) of Thick-Wall Alloy 600 Materials (MRP-55),” Revision 1, 1006695, Palo Alto, CA, 2002.

This page intentionally left blank

Nuclear Engineering Division
Argonne National Laboratory
9700 South Cass Avenue, Bldg. 208
Argonne, IL 60439

www.anl.gov

Argonne
National
Laboratory is a U.S. Department of Energy
laboratory managed by UChicago Argonne, LLC